Supporting Information

Immobilization of Rh(I) precursor in Porphyrin Metal-Organic Framework - Turning on Catalytic Activity

Anna M. Szczepkowska[a], Mateusz Janeta[a], Miłosz Siczek[a], Włodzimierz Tylus[b], Anna M. Trzeciak[a], Wojciech Bury[a]*

[a] Faculty of Chemistry, University of Wrocław, F. Joliot-Curie 14, 50-383 Wrocław, Poland

[b] Department of Advanced Material Technologies, Faculty of Chemistry, Wrocław University of Science and Technology, Wybrzeże Wyspiańskiego 27, 50-370 Wroclaw, Poland

*corresponding author: wojciech.bury@chem.uni.wroc.pl

Table of Contents

S1. Materials

Propionic acid (Sigma-Aldrich, ≥99.5%), benzoic acid (Acros, 99%), hydrochloric acid (HCl, Chempur, 36–38 %), glacial acetic acid (CH_3COOH, Eurochem, analytical grade), methyl *p*-formylbenzoate (Fluorochem, 98%), pyrrole (TCI, >99%), potassium hydroxide (KOH, Eurochem, analytical grade), di-*μ*-chloro-tetracarbonyldirhodium(I) ($[Rh(CO)_2Cl]_2$, Sigma-Aldrich, 97%), anhydrous sodium acetate (CH_3COONa, Eurochem, anhydrous), magnesium sulfate ($MgSO_4$, Fluorochem, anhydrous), zirconium(IV) chloride ($ZrCl_4$, Merck, 98%), 4-phenylboronic acid (Fluorochem, 98%), potassium carbonate (K_2CO_3, Chempur, 99%), tetrakis(triphenylphosphine)palladium(0) ($Pd(PPh_3)_4$, Sigma-Aldrich, 99%), methyl bromobenzoate (Fluorochem, 99%), sulfuric acid (Eurochem, 95%), hydrogen peroxide (JT Baker, 30-32%), 1-octene (Fluka, ≥97%), styrene (Alfa Aesar, 99.5%), cyclohexene (Roth, ≥99%), 2-cyclohexen-1-one (Sigma-Aldrich, ≥95%), were used without further purification.
Solvents: methanol (Chempur, 99%), dichloromethane (VWR, 99%), chloroform (CHEMSOLUTE, 99%), tetrahydrofuran (Eurochem, analytical grade), N,N-dimethylformamide (Chempur, 98%), N,N-diethylformamide (Fluka, >99%), toluene (Stanlab Sp. J., 98%), acetone (Chempur, 98%), n-hexane (Witko, 95%), deuterated chloroform ($CDCl_3$, stab. with Ag, Sigma-Aldrich, ≥99.8 atom% D), deuterated dimethylsulfoxide (DMSO-d_6, Deutero, 99.8 atom% D), deuterated sulfuric acid (D_2SO_4, Sigma-Aldrich, 96-98% solution in D_2O, 99.5 atom% D), were used as received. Toluene and CH_2Cl_2 used in catalytic or post-synthetic metalation reactions were purified and dried by using a solvent-purification system that contained activated alumina.

S2. Methods

^1H NMR spectra in solutions were recorded using a Bruker Avance 500 spectrometer equipped with broadband inverse gradient probe heads. Spectra were referred to the residual solvent signals $(CD_3)_2SO$, 2.50; $CDCl_3$, 7.26 as an internal reference. For NMR sample preparation, the ligand was dissolved in 0.6 mL of $CDCl_3$, a MOF sample was dissolved in a few drops of D_2SO_4 by sonication. The obtained solution was then mixed with d_6-DMSO and used for NMR measurement.
Preparative separations were performed on a CombiFlash EZ Prep System. Flash chromatography separations were performed on silica gel grade 60, 40–63 μm mesh (Fluorochem).
Optical emission spectrometry with excitation by argon inductively coupled plasma (ICP-OES) technique were performed using the Thermo Fisher Scientific iCAP 7400 DUO analyzer.
Infrared spectra were recorded at different temperatures using a Nicolet iS50 FT-IR (Thermo Scientific). The DRIFTS spectra were measured using a Praying Mantis DRIFTS accessory. The spectra of samples are in the 4000-550 cm^{-1} range. The spectra are averaging from 128 scans and include atmospheric correction. The spectral resolution was 4 cm^{-1}. The spectra were collected in a KBr mixture under N_2 purge. KBr was utilized as the background. Variable-temperature DRIFTS were collected using high temperature reaction chamber (Harrick Scientific Products Inc), accessory with temperature control performed with EZ-ZONE software with a heating step set to 1 °C/min under the N_2 purge.
Thermogravimetric and differential thermal analyses (simultaneous TG-DTA) were recorded on a Setaram SETSYS 16/18 instrument. Samples for thermogravimetric characterization were placed in alumina crucibles in synthetic air (O_2:N_2 = 20:80) (flow rate: 1 dm^3/h) at heating rate 5 ºC/min, samples were studied between 30 and 1000 ºC.

SEM images were collected on a Hitachi S-3400N-II variable-pressure scanning electron microscope. Samples were sputter-coated with 7 nm Au to facilitate viewing by SEM. Energy dispersive X-ray spectra (EDS) were obtained using a EDS Thermo Scientific Ultra Dry system. All gas sorption isotherms were measured on a Micromeritics ASAP 2020. Prior to the measurements, the samples were degassed at 120 °C for 24 h. Adsorption isotherms were measured at 77 K using a liquid nitrogen bath.

Powder XRD data were collected on Bruker D8 ADVANCE diffractometer equipped with a copper lamp (CuKα radiation, λ = 1.5406 Å) at 30 kV and 40 mA with a slit of 0.1°. Standard measurements were done 2θ range of 4°-40° with a 2θ step of 0.008° and a counting time of 0.5 s.

Single-crystal diffraction data were collected on a Rigaku Oxford Diffraction XtaLAB Synergy-R DW diffractometer equipped with a HyPix ARC 150° Hybrid Photon Counting (HPC) detector using Mo Kα (λ = 0.71073 Å) for **Rh/NU-1102(a)** and Cu Kα (λ = 1.54184 Å) for **Rh/PCN-222(a)** at 100 K. Diffraction data for **1c** were collected on a Kuma KM4 diffractometer equipped with Sapphire CCD detector at 100 K using Mo Kα (λ = 0.71073 Å). Data were processed using the CrysAlisPro software. The structures were solved by direct methods using SHELXS and refined by full-matrix least-squares methods based F^2 using SHELXL. For all structures, H atoms bound to C atoms were placed in the geometrically idealized positions and treated in riding mode, with C-H = 0.95 Å and $U_{iso}(H) = 1.2U_{eq}(C)$ for C-H groups, and C-H = 0.98 Å and $U_{iso}(H) = 1.5U_{eq}(C)$ for CH_3 groups. Diffraction data for **1c** was insufficient (R_{int}=0.2437) for publication and only indicative model of the structure has been obtained (chemical formula $C_{56}H_{36}N_4O_{12}Rh_2$•0.3($CHCl_3$), space group P21/c, a=10.301(2) b=29.369(6) c=10.680(2) β=104.88(2))

XPS spectra were recorded on a SPECS UHV/XPS/AES system equipped with a hemispherical PHOIBOS 100 analyzer operating in the fixed analyzer transmission (FAT) mode and a dual Mg/Al X-ray source, Mg-Kα X-ray source excitation (1253.6 eV) was operated at 250 W and 12 kV. The base pressure in the analysis chamber was less than 5×10^{-10} mbar. The spectrometer energy scale was calibrated with Au 4*f 7/2*, Ag 3*d 5/2*, and Cu 2*p 3/2* lines at 84.2, 367.9, and 932.4 eV, respectively. The binding energies were calibrated using carbon C 1s (C-C, C-H in aromatic) with BE at 284.8 eV as a reference. Spectra were processed and fitted by SPECLAB2 and CasaXPS v.2.3.19 software using Gaussian-Lorentzian curve profile and Shirley baseline. In deconvolution of the spectra for 3d orbitals, the area ratio $3d_{5/2}$:$3d_{3/2}$ was always 3:2. Zr $3d_{5/2}$-$3d_{3/2}$ splitting was equal to 2.43 eV while for Rh3d doublet 4.71 eV. Due to the Coster-Kronig effect, the $Rh3d_{3/2}$ component was broadened in compare to $Rh3d_{5/2}$.

GC-FID and GC/MS Spectra of the organic products were performed using the HP 5890 (Hewlett Packard) instrument with mass detector 5971 A. Capillary column HP 5 was used with a non-polar liquid phase containing 95% of dimethyl- and 5% of diphenylpolysiloxane.

S3. Synthesis of prolinkers and MOFs

S3.1. Synthesis of *meso*-tetrakis(4-methoxycarbonylphenyl)porphyrin (H_2TMCPP, 1a)

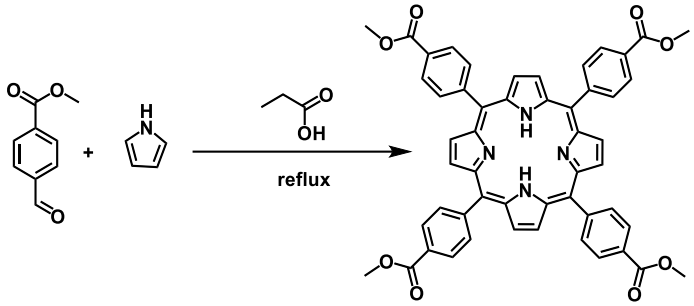

Scheme S1. Synthesis of **1a**.

The synthesis was carried out according to literature procedure.[1] To 500 mL two necked flask with refluxed propionic acid (270 mL) were added methyl *p*-formylbenzoate (18.6 g, 0.113 mol) and pyrrole (8.0 mL, 0.116 mol), and left refluxed for 12 h in darkness. The resulting mixture was cooled to room temperature and filtered. Collected purple solid was washed with water (3 L) to neutral pH and then with mixture H_2O/CH_3OH (1:1, 300 mL), and CH_3OH (2 L). Purple crystals were collected by recrystallization in CH_2Cl_2 (4.17 g, 4.92 mmol, 17.4% yield). ^{1}H NMR (500 MHz, $CDCl_3$, 300 K) δ 8.82 (s, 8H), 8.45 (d, 8H), 8.29 (d, 8H), 4.11 (s, 12H), -2.80 (s, 2H).

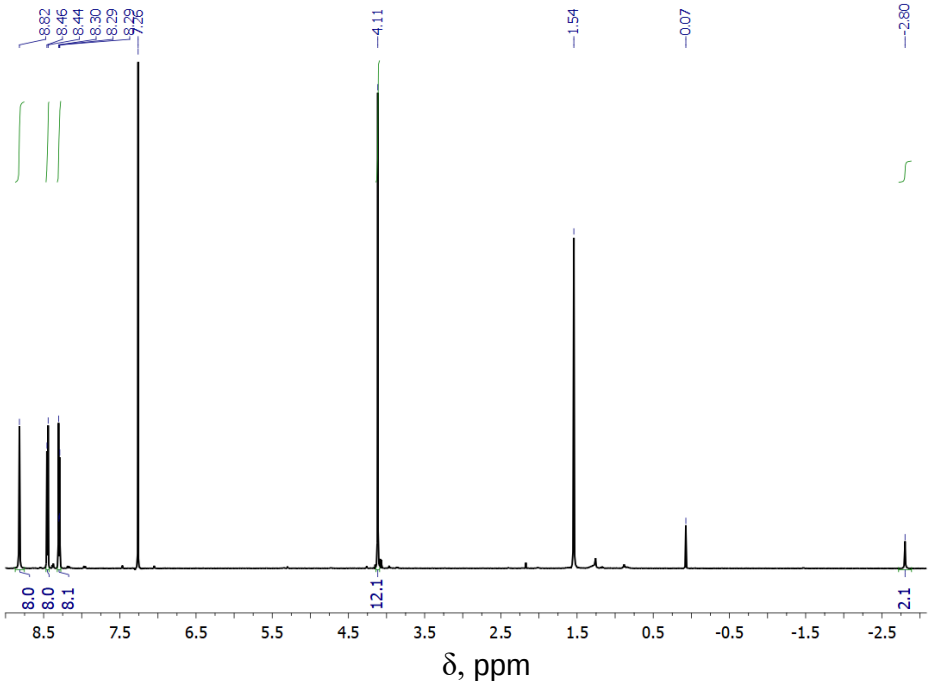

Figure S1. ^{1}H NMR spectrum of **1a**.

S3.2. Synthesis of *meso*-tetrakis(4-carboxyphenyl)porphyrin (H_2TCPP, 1b)

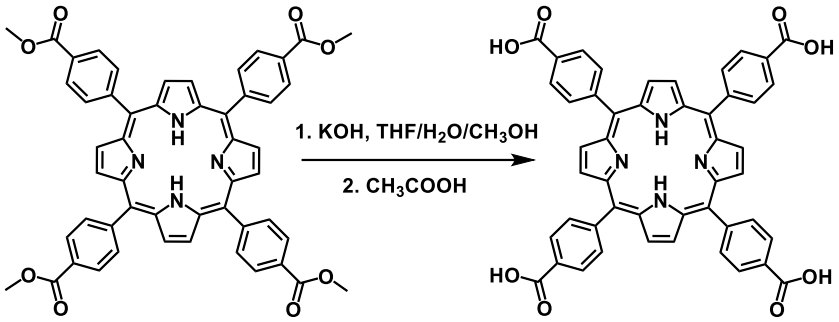

Scheme S2. Synthesis of **1b**.

The synthesis was carried out according to literature procedure.[1] To a 500 mL round bottom flask were added **1a** (2 g, 2.362 mmol), THF (70 mL), CH_3OH (70 mL) and solution of KOH (7 g, 0.125 mol) in water (70 mL), and left refluxed for 12 h. The mixture was cooled down and concentrated to evaporate organic solvents. To homogeneous solution CH_3COOH was added to adjust the pH to 4. The resulting precipitate was filtered and washed with water to neutral pH. Purple crystals were collected by dissolution of product in DMF and precipitation by $CHCl_3$ (1.65 g, 2.09 mmol, 88.3% yield). ^{1}H NMR (500 MHz, DMSO-d_6, 300 K) δ 13.31 (s, 4H), 8.86 (s, 8H), 8.38 (d, 8H), 8.33 (d, 8H), -2.93 (s, 2H).

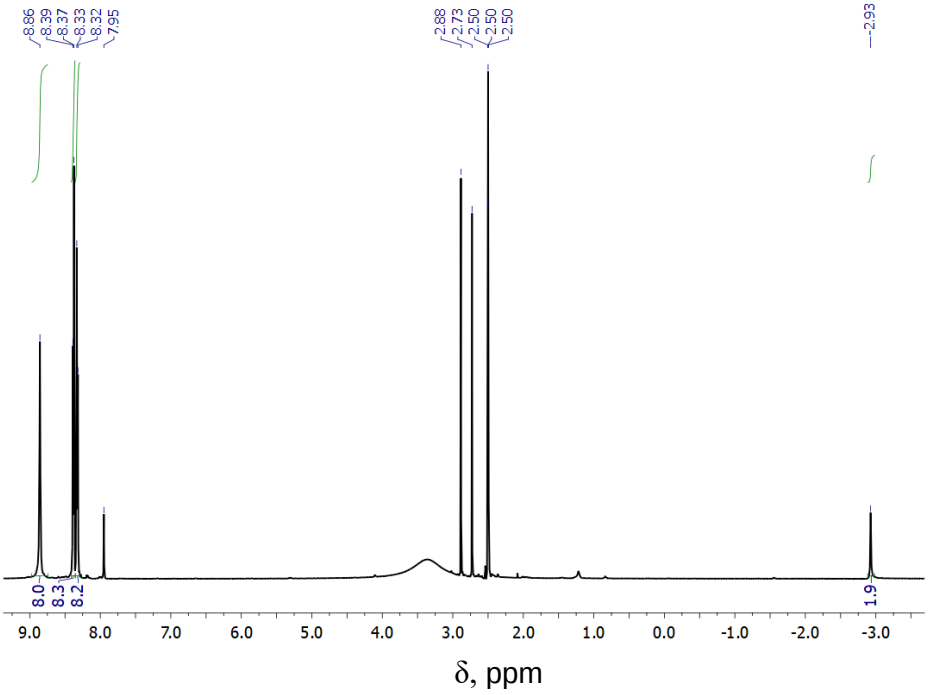

Figure S2. ^{1}H NMR spectrum of **1b**.

S3.3. Synthesis of (TMCPP)$Rh_2(CO)_2$, (1c)

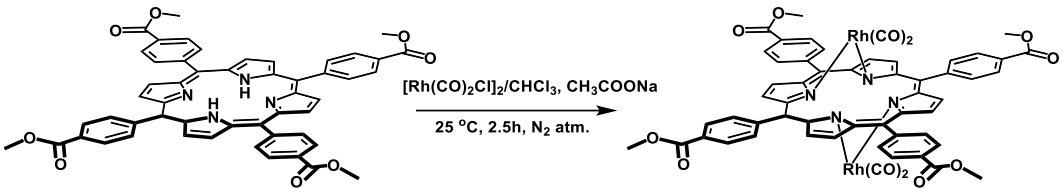

Scheme S3. Synthesis of **1c**.

Crystals of **1c** were obtained by crystallization from $CHCl_3$ (0.060 g, 90% yield). ^1H NMR (500 MHz, $CDCl_3$, 300 K) δ 8.72 (d, 4H), 8.56 (d, 4H), 8.49 (dd, 8H), 8.39 (dd, 8H), 4.12 (d, 12H).

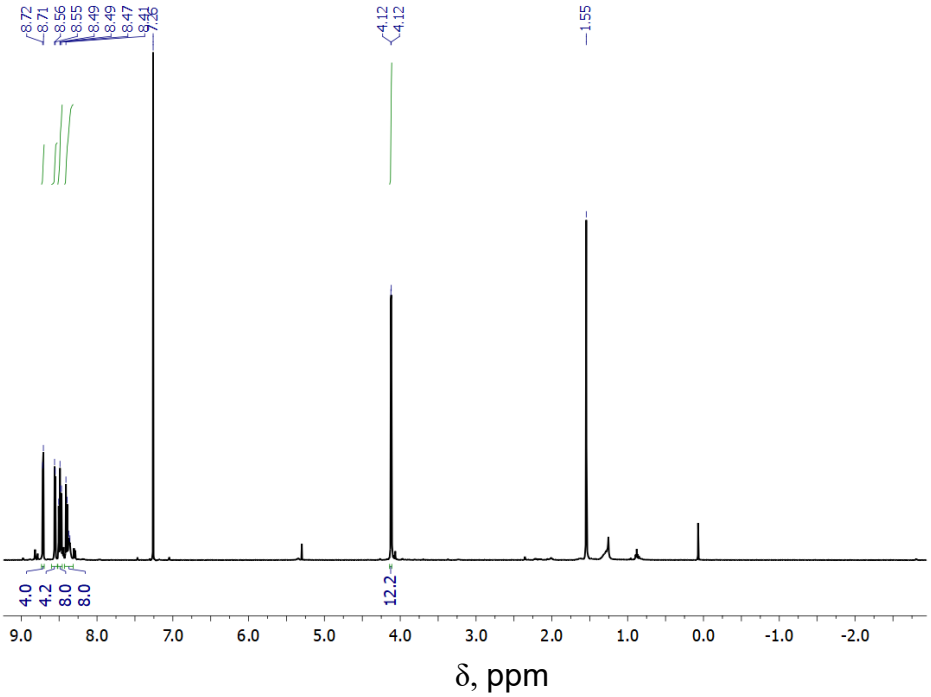

Figure S3. ^1H NMR spectrum of **1c**.

S3.4. Synthesis of PCN-222

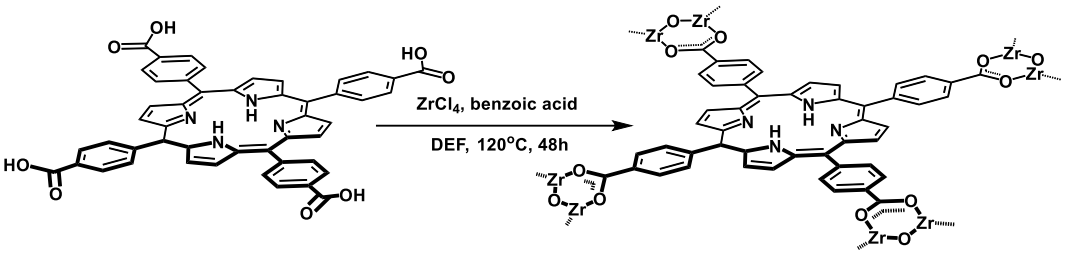

Scheme S4. Synthesis of **PCN-222**.

The synthesis was carried out according to literature procedure.[1] To a 20 mL glass vial were added $ZrCl_4$ (75 mg, 0.320 mmol), **1b** (50 mg, 0.063 mmol), benzoic acid (2.7 g, 0.022 mol) and N,N-diethylformamide (8 mL). The mixture was sonicated until a homogeneous slurry was obtained. The vial was sealed and placed in the oven at 120 °C for 48 h. After cooling down, the mother liquor was removed and purple crystals were washed with fresh DMF (8 mL) 3 times and left for 24 h. Then the solvent was exchanged with acetone and the washing procedure was repeated (3×8 mL, left overnight). Prior other studies acetone was removed, and purple crystals were dried in oven at 60 ˚C for 24 h (33 mg, 43 % yield). ^{1}H NMR (500 MHz, DMSO-d_6, 300 K) δ 8.80 (t, 16H), 8.61 (d, 8H), 7.89 (m, 4H), 7.58 (m, 2H), 7.45 (m, 4H). For further research dried material was not activated, therefore peaks from benzoic acid can be found in the spectrum.

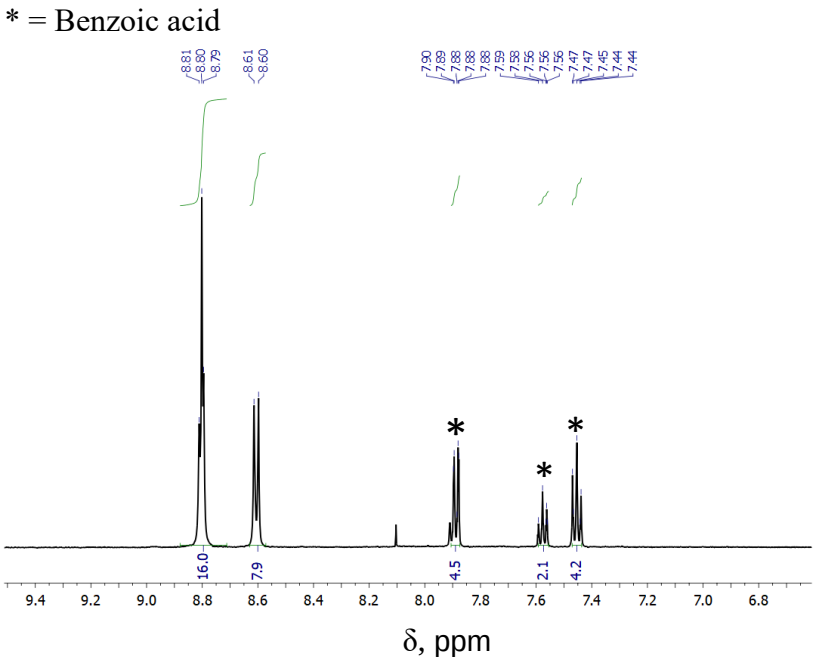

Figure S4. ^{1}H NMR spectrum of **PCN-222**.

S3.5. Synthesis of Rh/PCN-222.

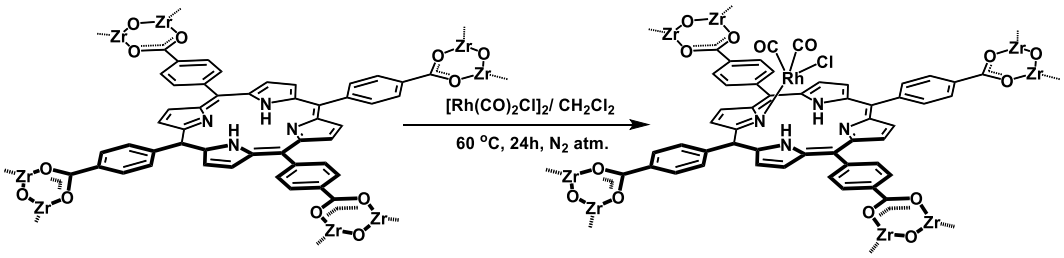

Scheme S5. Synthesis of **Rh/PCN-222**, n = 2 or 1.

^{1}H NMR (500 MHz, DMSO-d$_6$, 300 K) δ 8.78 (m, 10H), 8.58 (d, 6H), 8.29 (m, 8H), 7.85 (d, 4H), 7.55 (t, 2H), 7.43 (t, 4H). Composition of rhodium in **Rh/PCN-222** was verified by ICP-OES study.

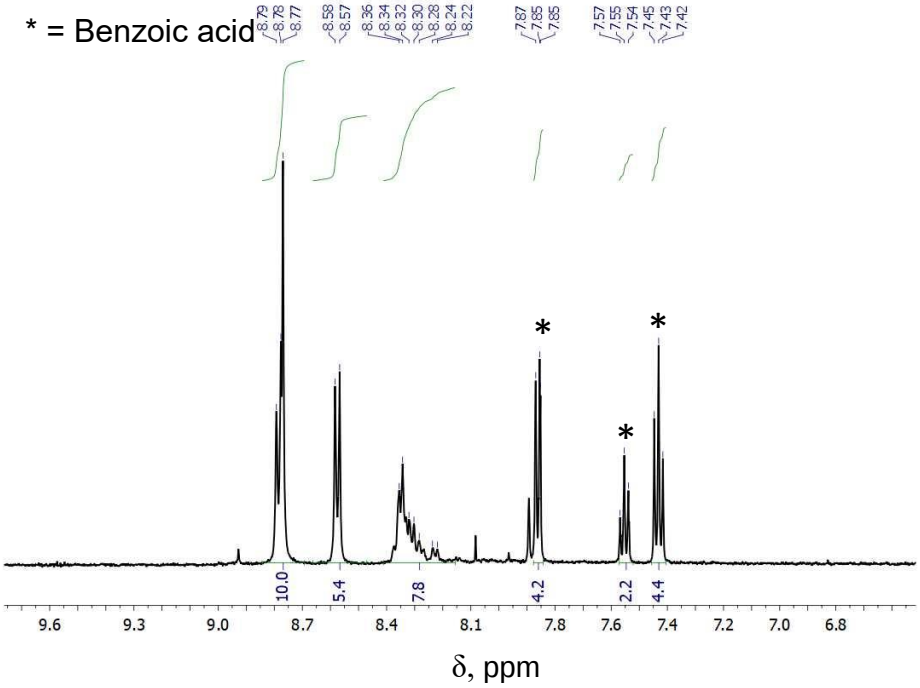

Figure S5. ^{1}H NMR spectrum of **Rh/PCN-222**.

Preparation of samples for ICP-OES study.

CAUTION: Piranha solution is a strong oxidizing and highly corrosive agent.

1.00 mg sample of tested MOF was placed in a vial. To another vial a piranha solution was added: 750 µL of sulfuric acid followed by 250 µL of hydrogen peroxide solution. Immediately the resulting solution (piranha solution) was transferred to the vial with weighed MOF crystals by a glass Pasteur pipette (solution changed color). The resulting mixture was heated at 100 °C until the solution was completely dissolved and was colorless. Then after cooling down the final solution was transferred into a 25 mL volumetric flask by a glass Pasteur pipette by thoroughly and repeatedly (5 times) washing the vial with distilled water. Volumetric flask with decomposed MOF was filled with distilled water to 25 mL. Prepared sample was measured on ICP-OES, and from the obtained results were calculated the metal to cluster and metal to metal ratio.

Table S1. Composition of **Rh/PCN-222** analyzed by ICP-OES.

MOF	formula	Rh/cluster	Rh/linker	Rh/Zr (mol/mol)
PCN-222	$Zr_6O_4(OH)_4(BA)_4L_2$	0	0	0
Rh/PCN-222 (theor.)	$Rh_2Zr_6O_4(OH)_4(BA)_4L_2$	2	1	0.33
Rh/PCN-222 (exp.)	$Rh_{2.43}Zr_6O_4(OH)_4(BA)_4L_2$	2.43	1.22	0.41

$L=H_xTCPP^{4-}$, x=2 for **PCN-222** and x = 1 for **Rh/PCN-222**;
$BA=PhCOO^-$;
theor. - theoretical results in which all porphyrin rings in the structure have coordinated one rhodium cation.

S3.6. Synthesis of methyl 4'-formyl-(1,1'-biphenyl)-4-carboxylate (FBPCMe).

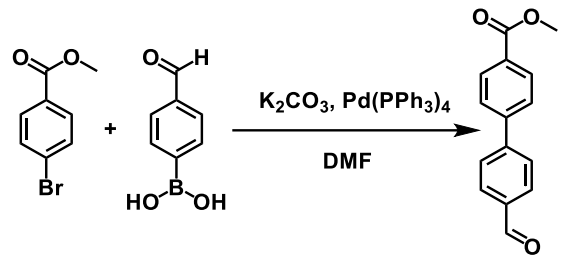

Scheme S6. Synthesis of **FBPCMe**.

The synthesis was carried out according to a reported modified procedure (US20110064694A1). To the Schlenk flask were added 4-phenylboronic acid (7.67 g, 51.15 mmol), K_2CO_3 (19.67 g, 142 mmol) and $Pd(PPh_3)_4$ (1.34 g, 1.16 mmol). Then under N_2 atmosphere were added degassed DMF (151 mL, degassed by bubbling N_2) and methyl bromobenzoate (10.0 g, 46.50 mmol). The resulting mixture was stirred and heated at 80 °C for 20 h and then 120 °C for 48 h. After cooling down and condensed to remove DMF, obtained product was extracted with CH_2Cl_2 and water. The resulting organic layer was dried with $MgSO_4$ and evaporated. The residue was chromatographed on silica gel with hexane to hexane/CH_2Cl_2 = 3:7 (10.76 g, 0.045 mol, 96.3% yield). ^{1}H NMR (500 MHz, $CDCl_3$) δ 10.08 (s, 1H), 8.15 (m, 2H), 7.98 (m, 2H), 7.79 (m, 2H), 7.71 (m, 2H), 3.96 (s, 3H).

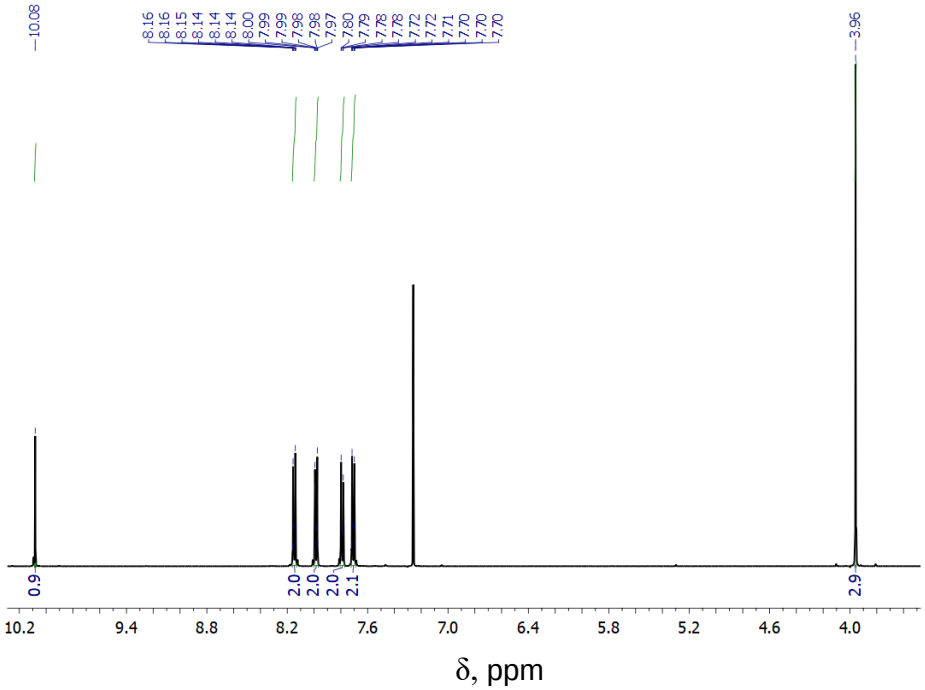

Figure S6. ^{1}H NMR spectrum of **FBPCMe**.

S3.7. Synthesis of *meso*-tetrakis-(4-methylcarboxybiphenyl)porphyrin (H_2TMCBPP, 2a).

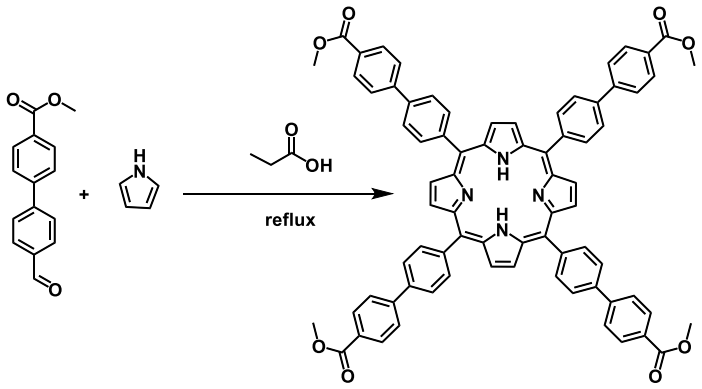

Scheme S7. Synthesis of **2a**.

The synthesis was carried out according to literature procedure.[2] To **FBPCMe** (5.30 g, 22.06 mmol) was added propionic acid (165 mL, 2.21 mol), stirred and heated to reflux. Pyrrole (1.53 mL, 22.06 mmol) was purified on silica gel, added to refluxed mixture and left in reflux for 20 h in darkness. The resulting mixture was cooled to room temperature, filtered and washed with water. The residue was chromatographed twice on silica gel with $CHCl_3$ to $CHCl_3/CH_3OH$=100:0.5, to separate the by-products soluble in $CHCl_3$. Obtained purple crystals were dried in oven at 100 ˚C for 24 h. (1. 62 g, 1.41 mmol, 26% yield). ^{1}H NMR (500 MHz, $CDCl_3$) δ 8.95 (s, 8H), 8.31 (m, 16H), 8.03 (m, 16H), 4.01 (s, 12H), -2.68 (s, 2H).

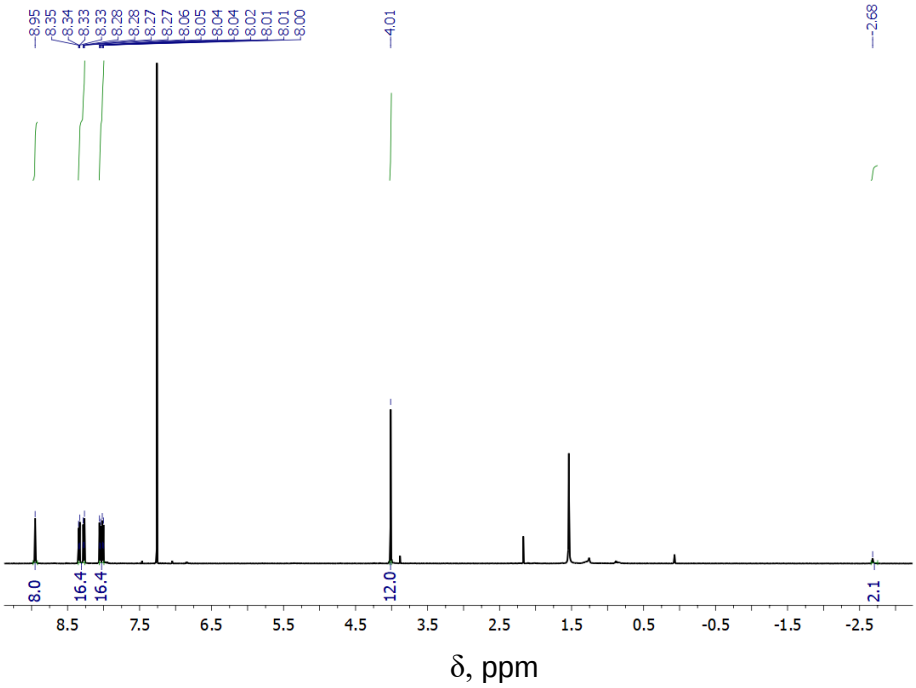

Figure S7. ^{1}H NMR spectrum of **2a**.

S3.8. Synthesis of *meso*-tetrakis-(4-carboxybiphenyl)porphyrin (H_2TCBPP, 2b).

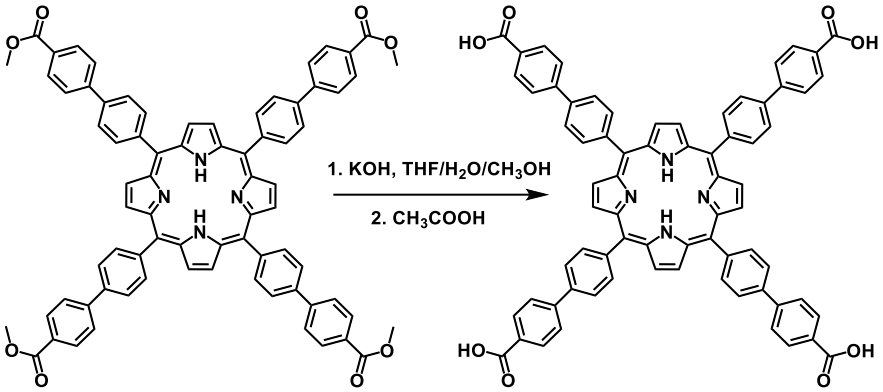

Scheme S8. Synthesis of **2b**.

The synthesis was carried out according to literature procedure.[2] To a 500 mL round bottom flask were added **2a** (0.63 g, 0.054 mmol), THF (78 mL), CH_3OH (53 mL) and solution of KOH (13.52 g, 0.241 mol) in water (78 mL), and left refluxed for 48 h. The mixture was cooled down and concentrated to evaporate organic solvents. To homogeneous solution 1M HCl was added to adjust the pH to 5. The resulting precipitate was filtered and washed with water to neutral pH. Purple crystals were collected by dissolution of product in DMF and precipitation by $CHCl_3$ (0.52 g, 0.47 mmol, 87.1% yield). ^{1}H NMR (500 MHz, DMSO-d_6, 300 K) δ 13.05 (s, 4H), 8.97 (s, 8H), 8.38 (d, 8H), 8.24 (d, 8H), 8.18 (s, 16H), -2.82 (s, 2H).

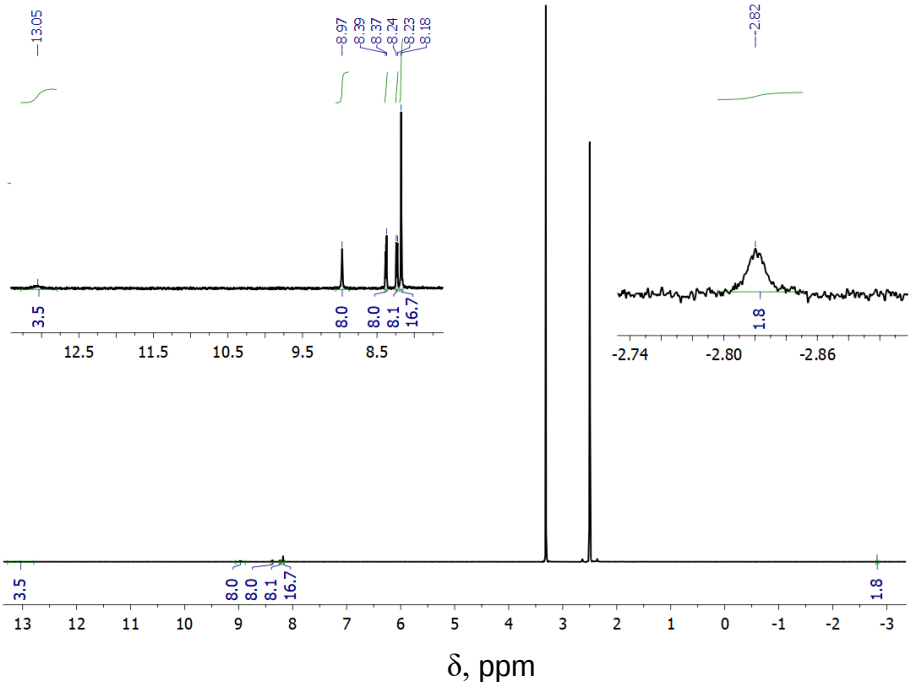

Figure S8. ^{1}H NMR spectrum of **2b**.

S3.9. Synthesis of NU-1102.

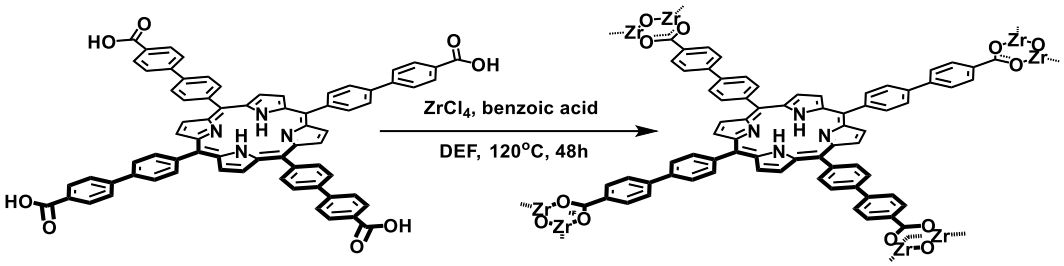

Scheme S9. Synthesis of **NU-1102**.

A 6 ml glass vial was charged with $ZrCl_4$ (0.375 g, 0.160 mmol), **2b** (0.059 g, 0.054 mmol) and DEF (4 mL). The mixture was sonicated until a homogeneous slurry was obtained. Next, benzoic acid (0.675 g, 5.5 mmol) was added to the vial and once again the mixture was sonicated until dissolved. The vial was sealed and placed in the oven at 120 °C for 3 days. After 3 days and cooling down to room temperature, the mother liquor was removed, and purple crystals were washed with fresh DMF (8 mL) 3 times and left overnight. Then DMF was exchanged with acetone three times every 24 h (3×8 mL). Purple crystals (cubic shaped) were isolated by removing the acetone and dried in oven at 60 ˚C for 24 h (19.21 mg, 36% yield). ^{1}H NMR (500 MHz, DMSO-d_6, 300 K) δ 8.80 (m, 16H), 8.46 (d, 8H), 8.17 (dd, 16H).

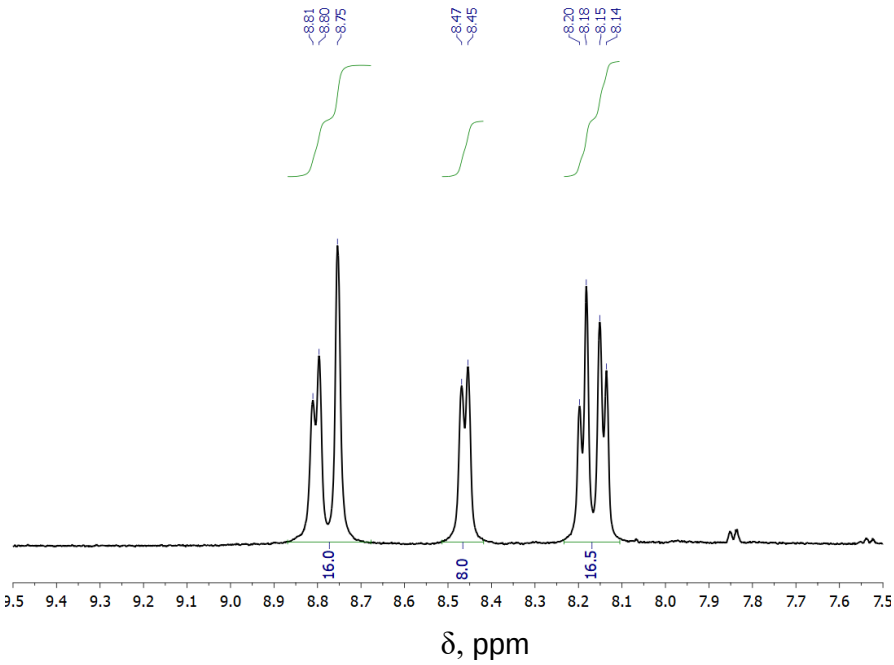

Figure S9. ^{1}H NMR spectrum of **NU-1102**.

S3.10. Synthesis of Rh/NU-1102.

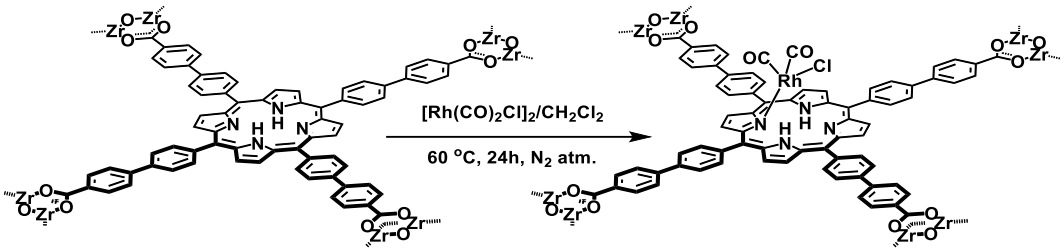

Scheme S10. Synthesis of **Rh/NU-1102**, n = 1 or 2.

^{1}H NMR (500 MHz, DMSO-d$_6$, 300 K) δ 8.81 (m, 12H), 8.49 (d, 6H), 8.34 (m, 2H), 8.18 (m, 20H). Composition of rhodium in **Rh/NU-1102** was verified with ICP-OES study.

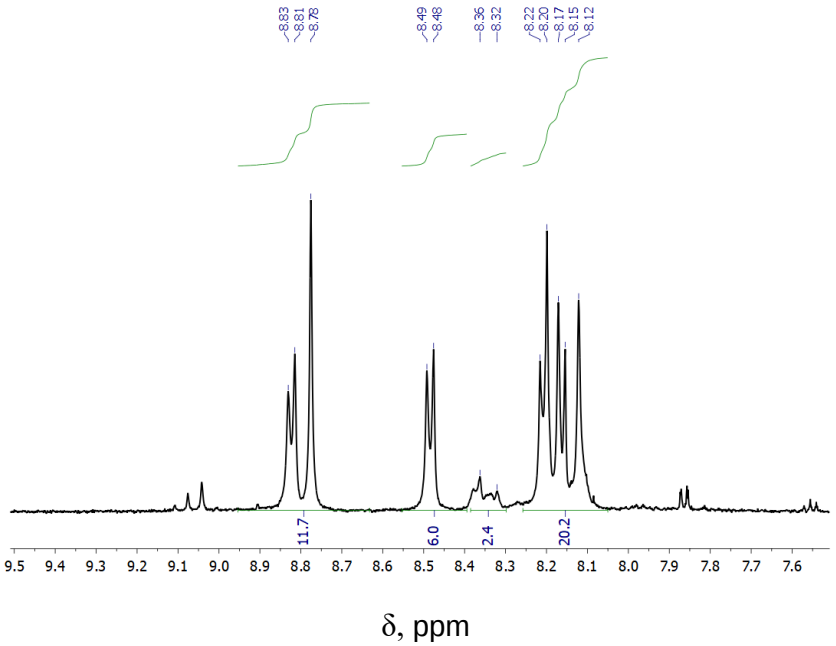

Figure S10. ^{1}H NMR spectrum **of Rh/NU-1102**.

Table S2. Composition of **Rh/NU-1102** analyzed by ICP-OES.

MOF	formula	Rh/cluster	Rh/linker	Rh/Zr (mol/mol)
NU-1102	$Zr_6O_4(OH)_4L_3$	0	0	0
Rh/NU-1102 (theor.)	$Rh_3Zr_6O_4(OH)_4L_3$	3	1	0.50
Rh/NU-1102 (exp.)	$Rh_{3.43}Zr_6O_4(OH)_4L_3$	3.43	1.14	0.58

L=H_xTCBPP $^{4-}$, x=2 for **NU-1102** and x=1 for **Rh/NU-1102**;
theor. - theoretical results in which all porphyrin rings in the structure have coordinated one rhodium cation.

S3.11. Reaction of 1a with $[Rh(CO)_2Cl]_2$ without a base

Schlenk flask was charged with **1a** (0.040 g, 0.050 mmol), $[Rh(CO)_2Cl]_2$ (0.010 g, 0.025 mmol) and CH_2Cl_2 (3 mL) under N_2 atmosphere. Then a solution was placed in a ThermoMixer (550 rpm) at 60 °C for 24 h. The resulting mixture was evaporated and the resulting post-reaction residue was checked by the ^1H NMR study.

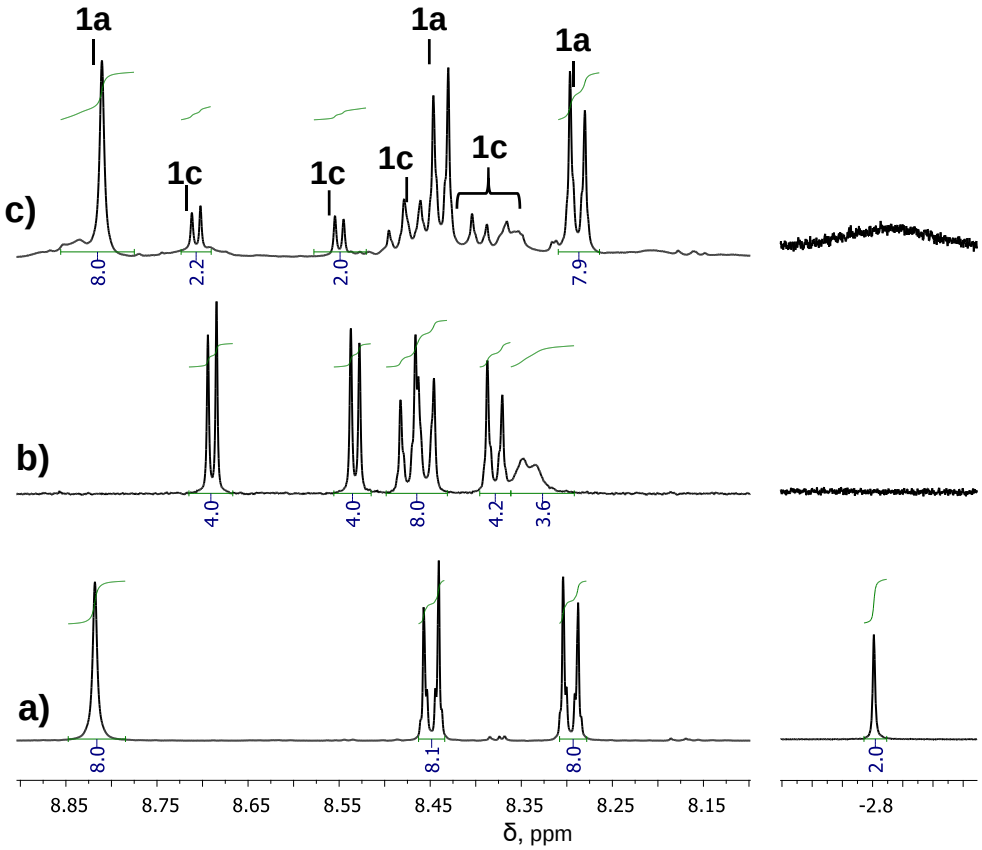

Figure S11. Comparison of ^1H NMR spectra of **1a** (a), **1c** (b) and post-reaction mixture of metalation **1a** by the same method as for **Rh/PCN-222** (c).

S4. Structural characterization of Rh/MOFs

S4.1.SEM images and EDS analysis.

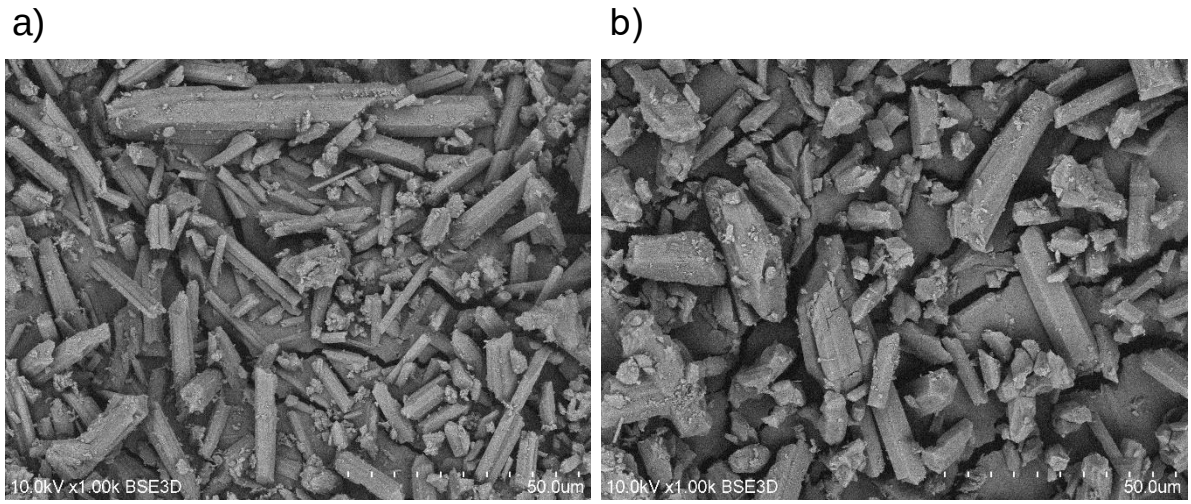

Figure S12. SEM images of: (a) **PCN-222**; (b) **Rh/PCN-222**.

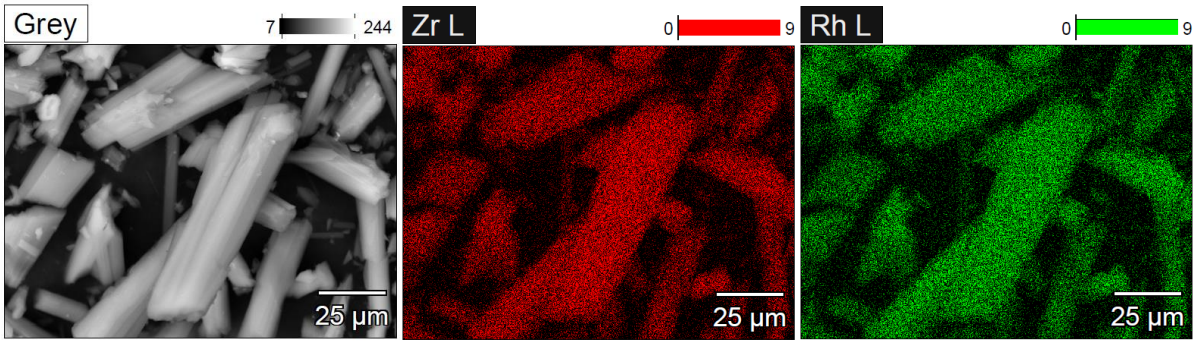

Figure S13. EDS mapping for Zr and Rh of **Rh/PCN-222**.

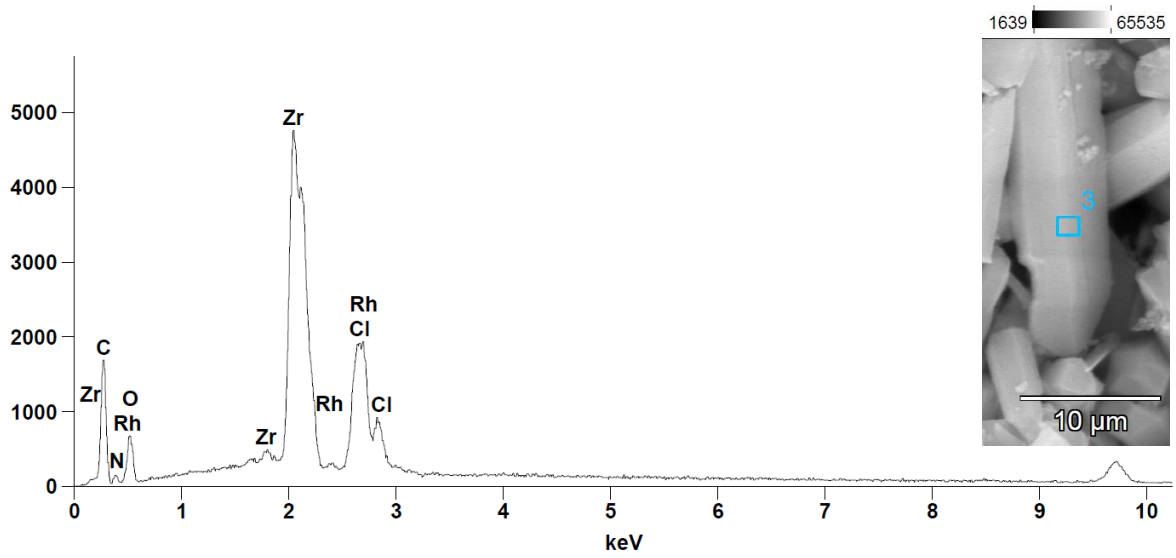

Figure S14. EDS spectrum of **Rh/PCN-222**, data collected from the area marked with blue frame.

Table S3. EDS analysis of **Rh/PCN-222** compared to ICP and XPS study (before and after catalysis).

Weight (%)	Zr	Rh	Cl	Rh/Zr
Rh/PCN-222 (EDS)	30.31	14.08	4.76	0.46
Rh/PCN-222 (ICP)				0.41
Atom (%)	Zr	Rh	Cl	Rh/Zr
Rh/PCN-222 (EDS)	7.67	3.16	3.10	0.41
Rh/PCN-222 (ICP)				0.36
Rh/PCN-222 (XPS)			3.45	0.40*
Rh/PCN-222 after catalysis (XPS)			3.39	0.38*

* for details see section 4.2

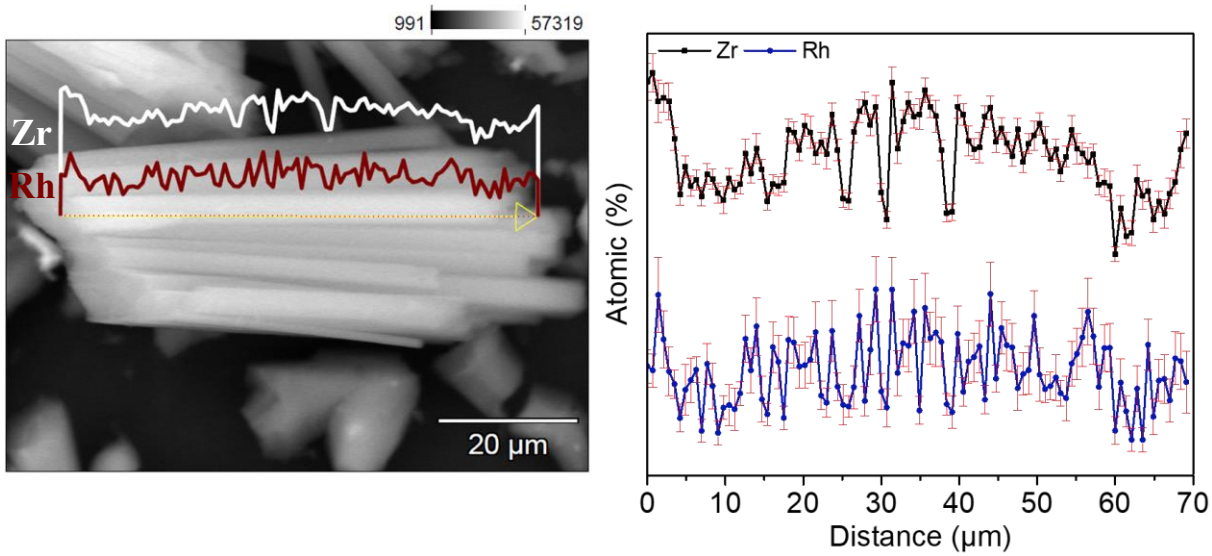

Figure S15. EDS profile for Zr and Rh across the crystal of **Rh/PCN-222**.

Table S4. EDS analysis of **Rh/PCN-222**, data averaged and collected from the line profile Figure S15.

Atom (%)	Rh/Zr
Rh/PCN-222 (EDS profile)	0.39 ± 0.01
Rh/PCN-222 (ICP)	0.36

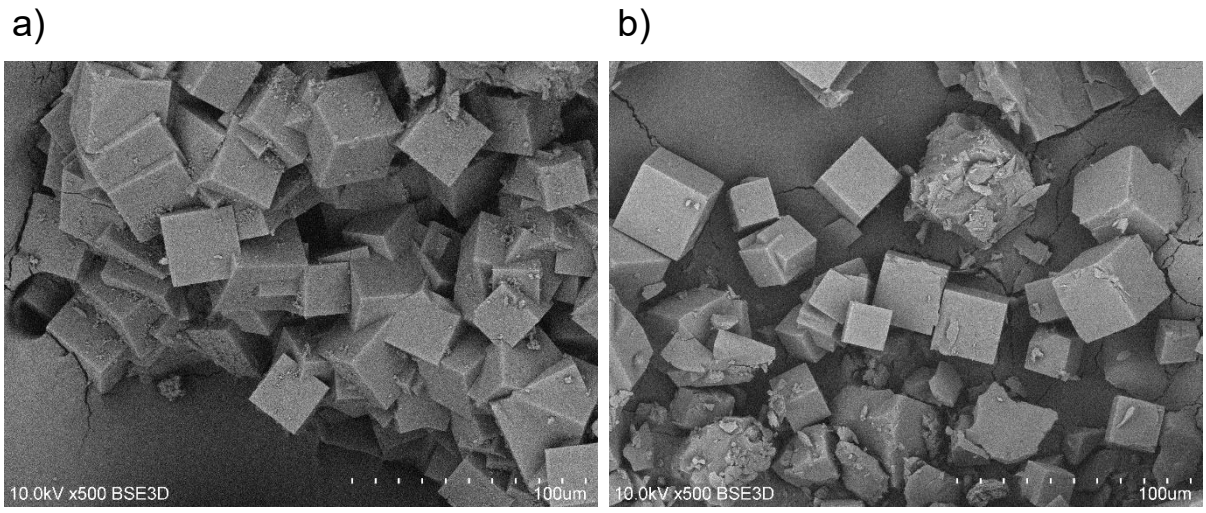

Figure S16. SEM images of: (a) **NU-1102**; (b) **Rh/NU-1102**.

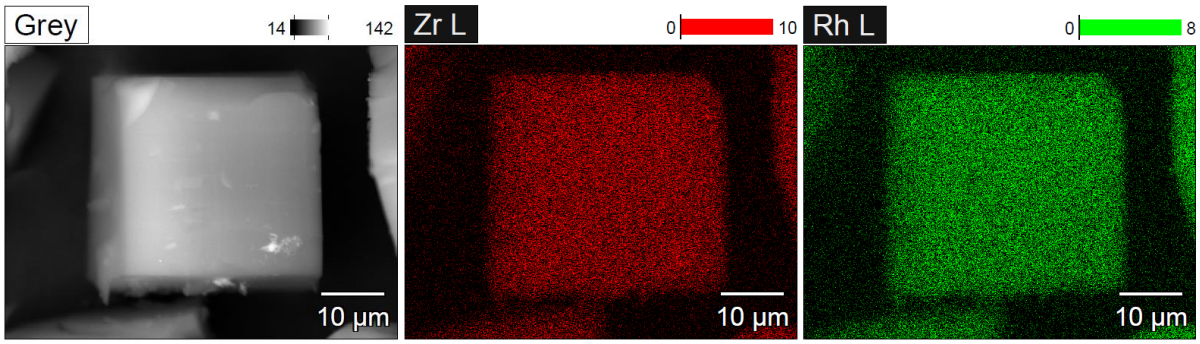

Figure S17. EDS mapping for Zr and Rh of **Rh/NU-1102**.

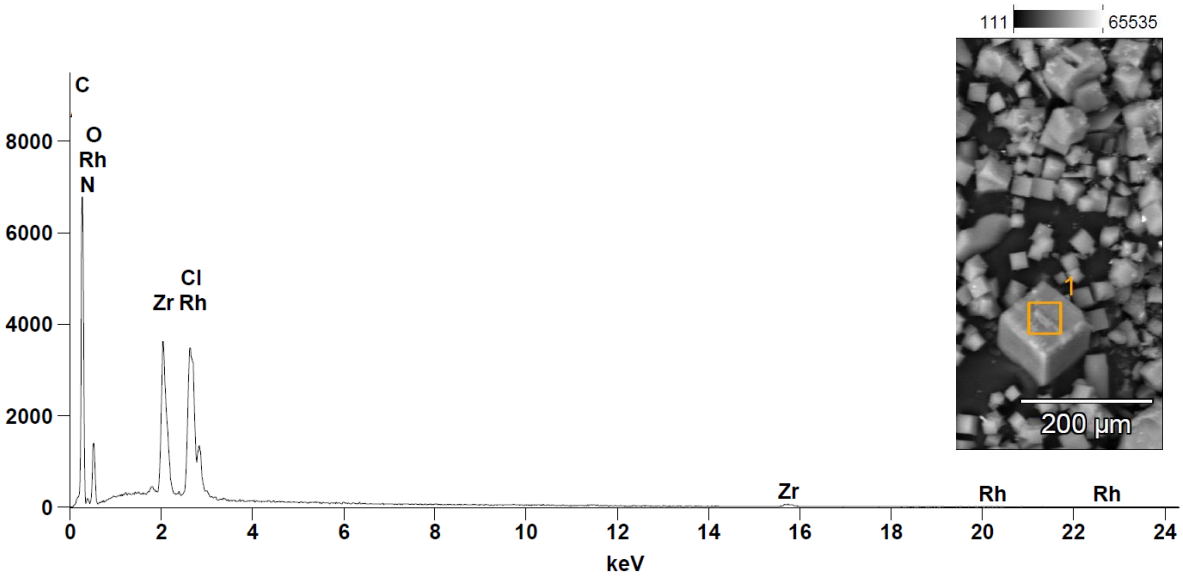

Figure S18. EDS spectrum of **Rh/NU-1102**, data collected from the area marked with orange frame.

Table S5. EDS analysis of **Rh/NU-1102** compared to ICP study, EDS data collected from the area marked with an orange frame Figure S4.7.

Weight (%)	Zr	Rh	Cl	Rh/Zr
Rh/NU-1102 (EDS)	10.64	9.85	4.57	0.93
Rh/NU-1102 (ICP)				0.58
Atom (%)	Zr	Rh	Cl	Rh/Zr
Rh/NU-1102 (EDS)	1.97	1.62	2.18	0.82
Rh/NU-1102 (ICP)				0.51

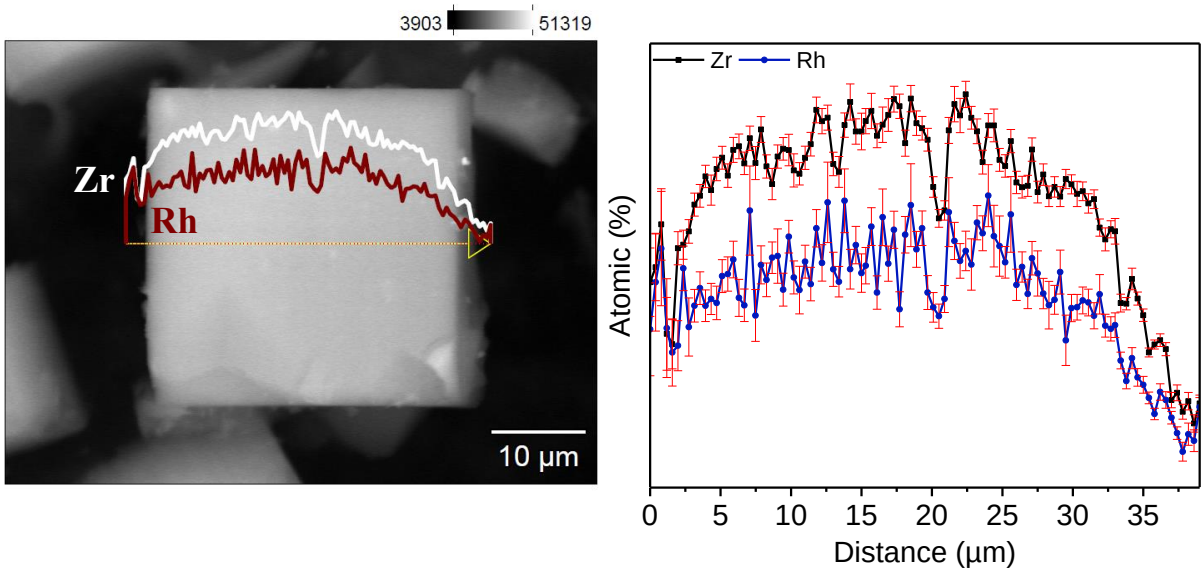

Figure S19. EDS profile for Zr and Rh across the crystal of **Rh/NU-1102**.

Table S6. EDS analysis of **Rh/NU-1102**, data averaged and collected from the line profile Figure S19.

Atom (%)	Rh/Zr
Rh/NU-1102 (EDS profile)	0.63 ± 0.04
Rh/NU-1102 (ICP)	0.51

S4.2. X-Ray Photoelectron Spectroscopy (XPS)

The binding energies of Rh(0), Rh(I), Rh (II) and Rh(III) available in publications and databases overlap.[3,4]

Table S7. XPS analysis of **Rh/PCN-222** before and after catalysis.

Atom (%)	Rh/Zr
Rh/PCN-222 (XPS, before catalysis)	0.40
Rh/PCN-222 (XPS, after catalysis)	0.38

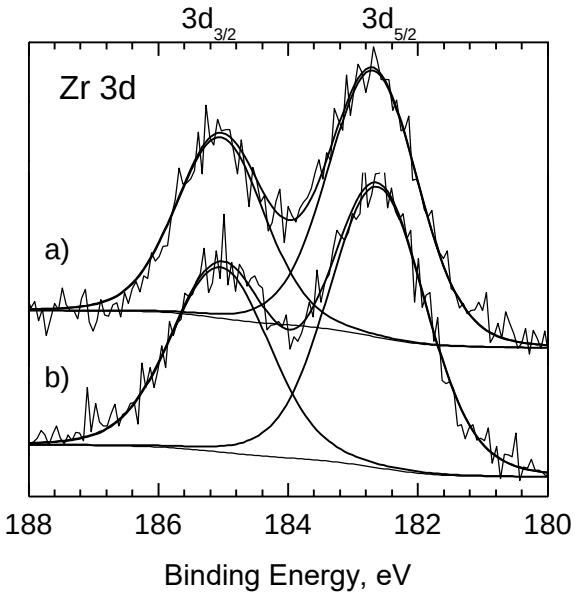

Figure S20. XPS Zr 3d core level for **Rh/PCN-222** before (a) and after catalysis (b).

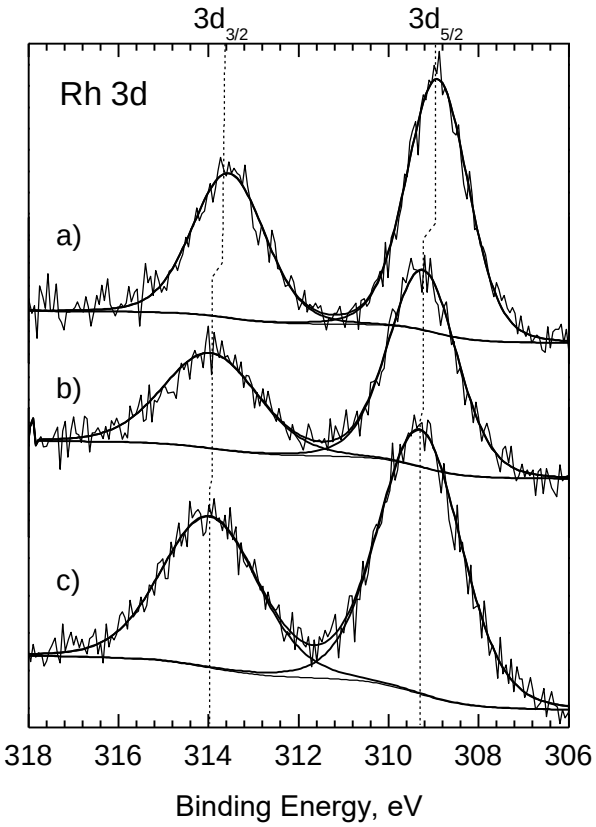

Figure S21. XPS Rh 3d core level for **1c** (a) and for **Rh/PCN-222** before (b) and after catalysis (c).

To further explore possible oxidation states of Rh in **1c** and **Rh/PCN-222** additional supplementary measurements were carried out. The samples were intentionally treated with an Ar^+ ion beam which resulted in the reduction of Rh(I) to Rh(0). Final Rh $3d_{5/2}$ peaks positions, after Ar^+ treatment for both samples was at ca. 307.6 eV. This value of binding energy is characteristic for Rh(0). The observed shifts of the binding energy for both samples were remarkably similar, without any intermediate steps which gives us a fair confirmation of the presence of Rh(I) in both samples (Figure S22 and S23).

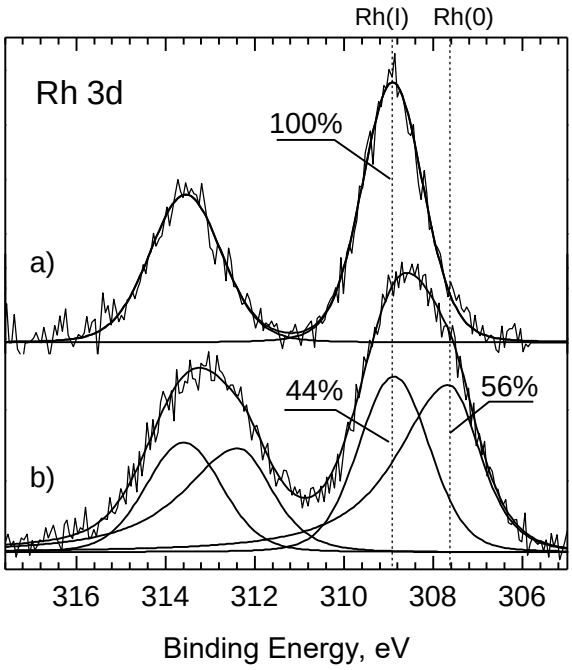

Figure S22. XPS Rh 3d core level for **1c** before (a), and after 1 min Ar^+ sputtering (2.5 keV, 4.5 μA/cm^2) (b). For Rh(0) the asymmetric peak shape was applied: LA (1.2, 3,2) [see: http://www.xpsfitting.com/search/label/Rhodium].

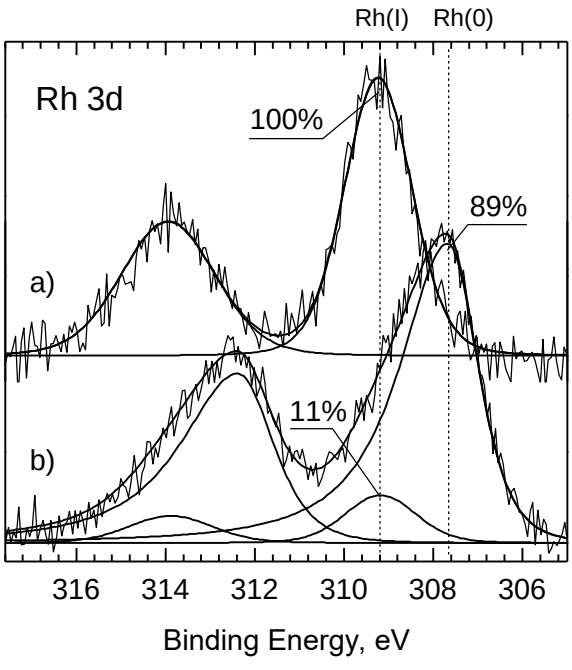

Figure S23. XPS Rh 3d core level for **Rh/PCN-222** before (a), and after 1 min Ar^+ sputtering (b). For Rh(0) the asymmetric peak shape was applied: LA (1.2, 3,2) [see: http://www.xpsfitting.com/search/label/Rhodium].

S4.3. Diffuse reflectance infrared Fourier transform spectroscopy (DRFITS).

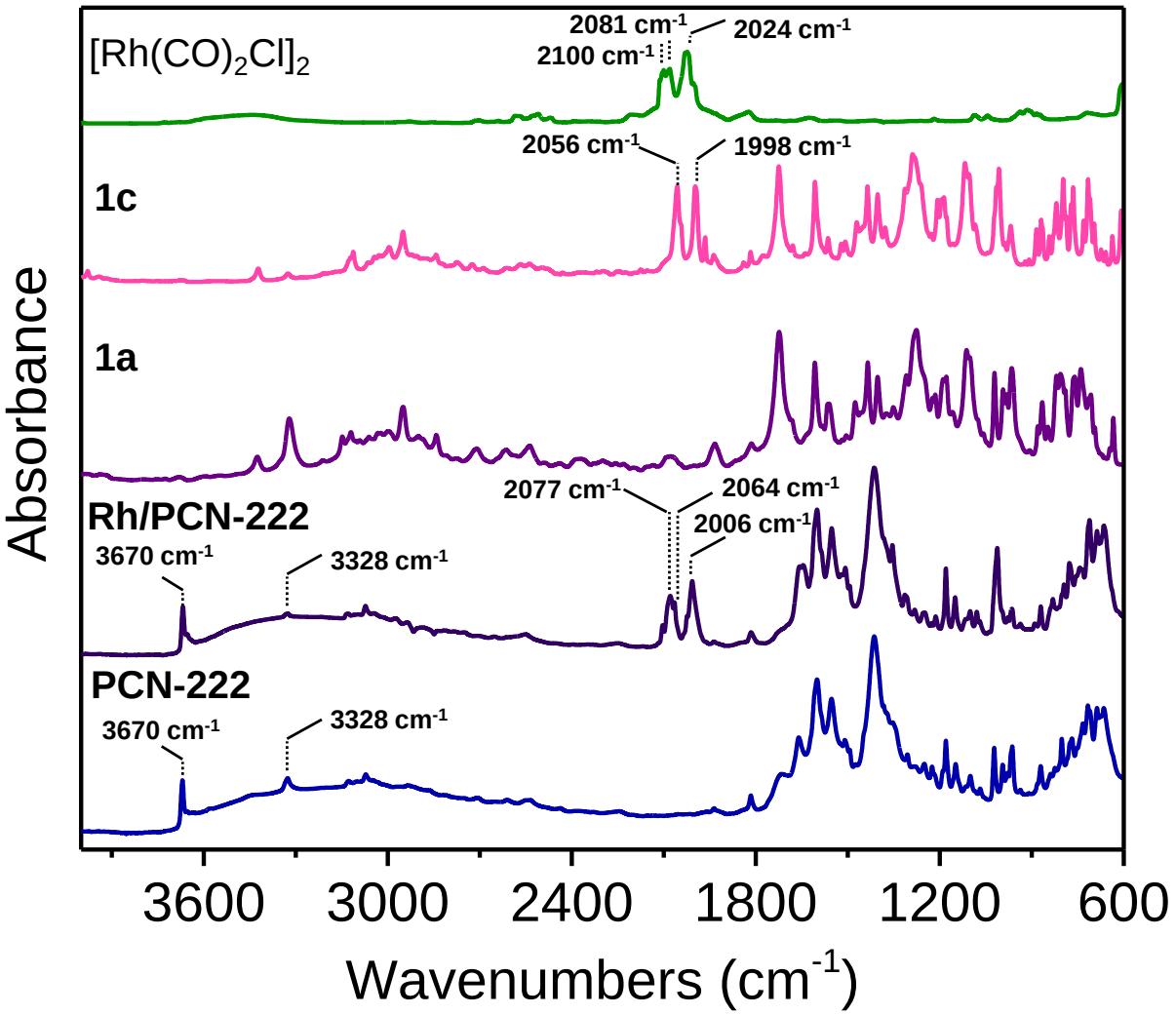

Figure S24. Comparison of DRIFTS spectra of **PCN-222**, **Rh/PCN-222**, **1a**, **1c** and $[Rh(CO)_2Cl]_2$ in the range of 4000-600 cm^{-1}.

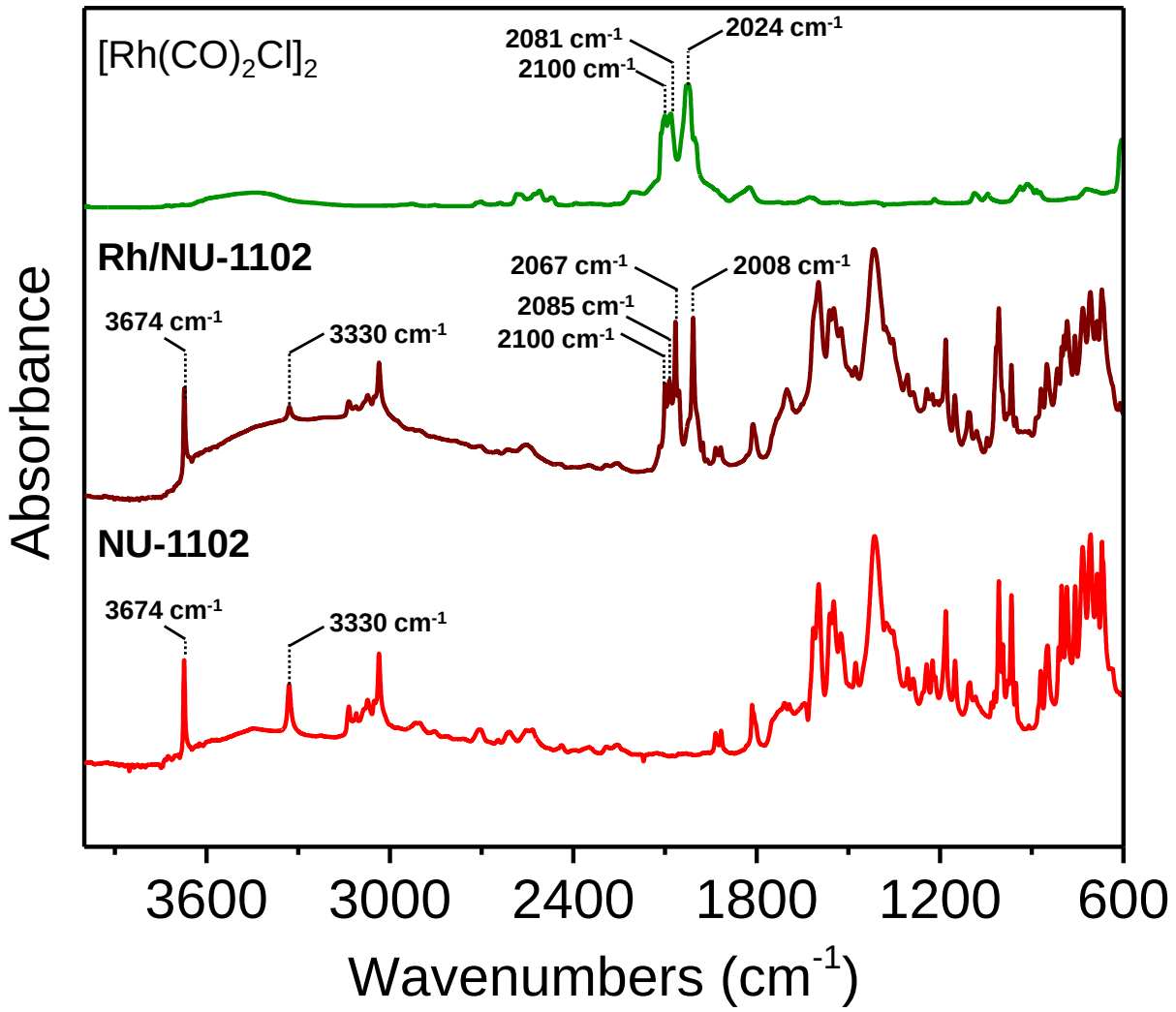

Figure S25. Comparison of DRIFTS spectra of **NU-1102**, **Rh/NU-1102** and $[Rh(CO)_2Cl]_2$ in the range of 4000-600 cm^{-1}.

S4.4. Single crystal X-ray diffraction studies.

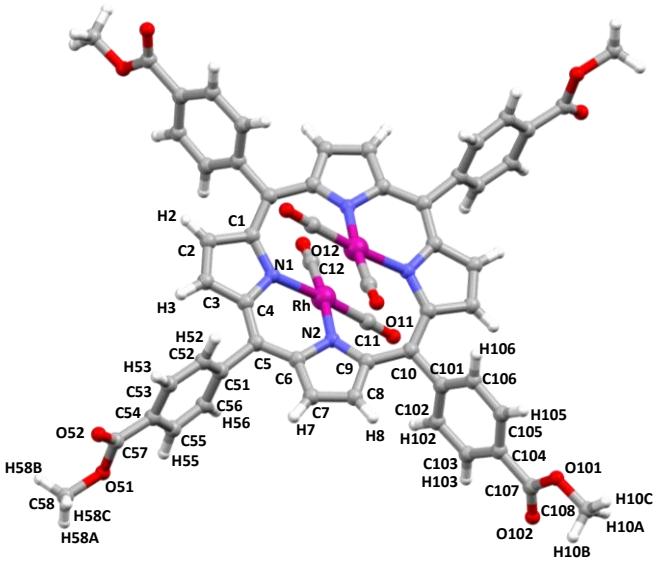

Figure S26. The molecular structure of **1c**.

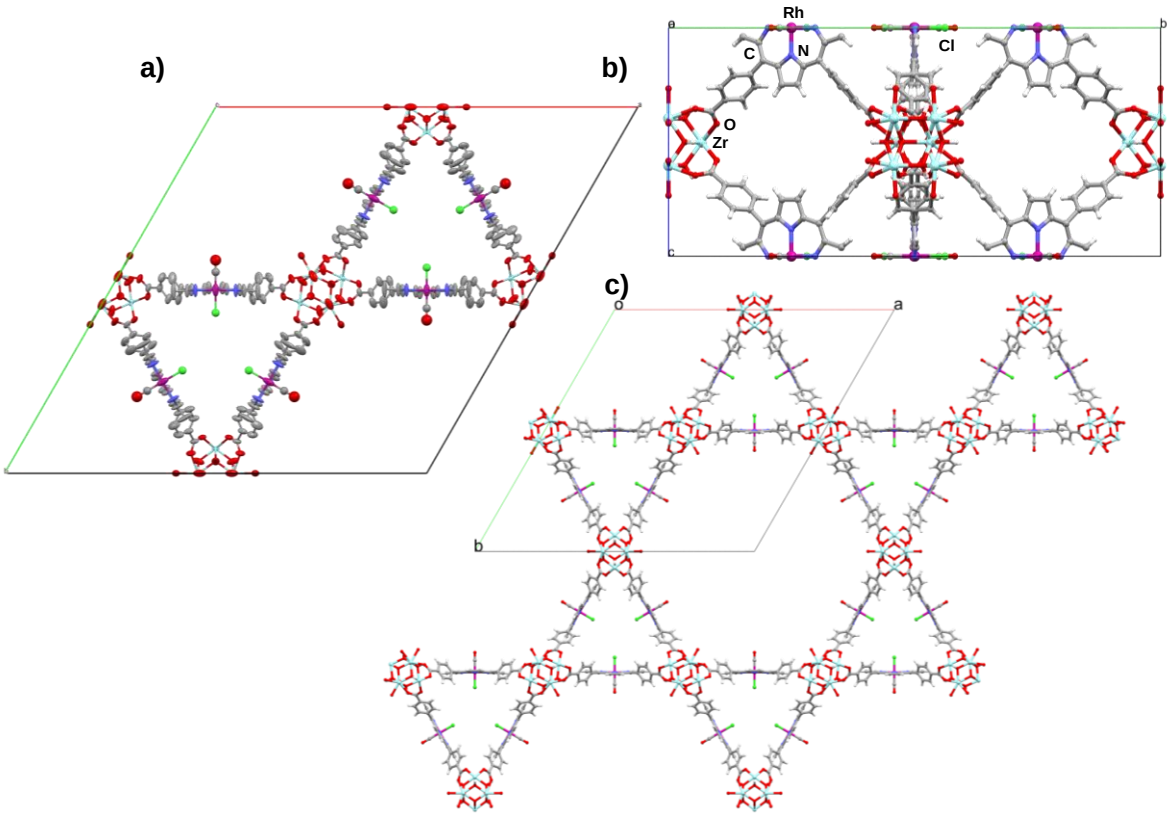

Figure S27. The crystal structure of **Rh/PCN-222(a)**. Ellipsoid style of crystal packing in the unit cell viewed along the *c*-axis, hydrogen atoms have been omitted for clarity (a), ball and stick style of crystal packing in the unit cell viewed along the *a*-axis or *b*-axis (b) and representation of the MOF topology (c).

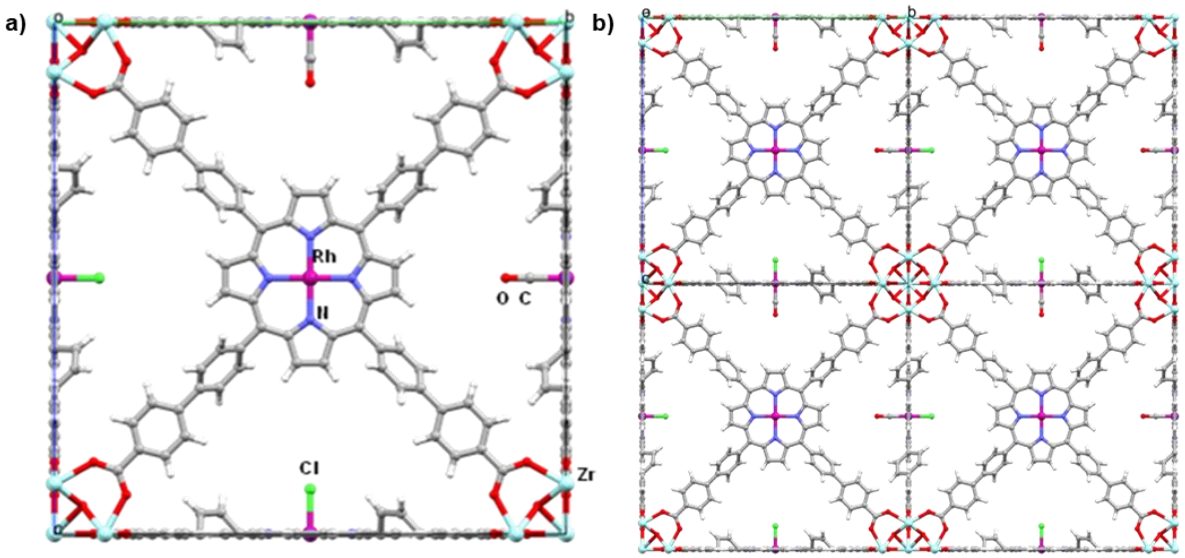

Figure S28. The crystal structure of **Rh/NU-1102(a)**. The ball and stick representation of the crystal packing viewed along the *a*-axis for: a) 1 unit cell, b) 4 neighbouring unit cells. The disordered parts of the structure have been omitted for clarity.

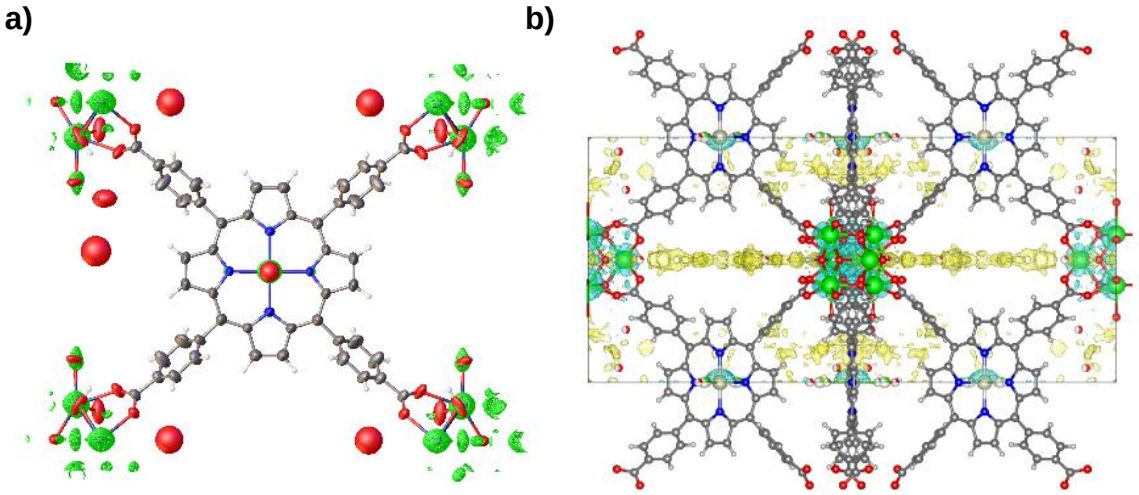

Figure S29. Perspective view of 3D electron density maps F_o (a) and (F_o–F_c) (b) of **Rh/PCN-222(a)** at 100 K. F_o–F_c maps are contoured at 0.6 e Å^3.

Table S8. Crystal data, data collection and structure refinement details for **Rh/PCN-222(a)** and **Rh/NU-1102(a)**.

	Rh/PCN-222(a)	**Rh/NU-1102(a)**
Chemical formula	$C_{97}H_{65}ClN_8O_{38}Rh_2Zr_6$	$C_{216.75}H_{124}Cl_{0.75}N_{12}O_{32.75}Rh_3Zr_6$•8($H_2O$)
Formula Mass	2727.06	4429.49
Crystal system	hexagonal	cubic
a(Å)	42.262(8)	25.388(3)
b(Å)	42.262(8)	25.388(3)
c(Å)	16.951(2)	25.388(3)
β(°)		
γ(°)	120	
Unit cell volume(Å^3)	26220(10)	16364(6)
Temperature(K)	100(2)	100(2)
Space group	*P*6/*mmm*	*Pm*-3*m*
No. of formula units per unit cell, *Z*	3	1
Radiation type	CuKα	MoKα
No. of reflections measured	121519	47220
No. of independent reflections	8665	3663
R_{int}	0.1078	0.0532
Final R_1 values ($I > 2\sigma(I)$)	0.0964	0.0901
Final $wR(F^2)$ values ($I > 2\sigma(I)$)	0.2784	0.2518
Final R_1 values (all data)	0.1356	0.1155
Final $wR(F^2)$ values (all data)	0.3173	0.3109
Goodness of fit on F^2	1.165	1.234

All data have been deposited with the Cambridge Crystallographic Data Centre CCDC 2051075 for **1c**, 2051076 for **Rh/PCN-222(a)** and 2051077 for **Rh/NU-1102(a)**. Copies of the data can be obtained free of charge on application to CCDC, 12 Union Road, Cambridge CB2 1EZ, UK (fax: +44 1223 336033; e-mail: deposit@ccdc.cam.ac.uk)

S4.5. Variable-temperature DRIFTS analysis.

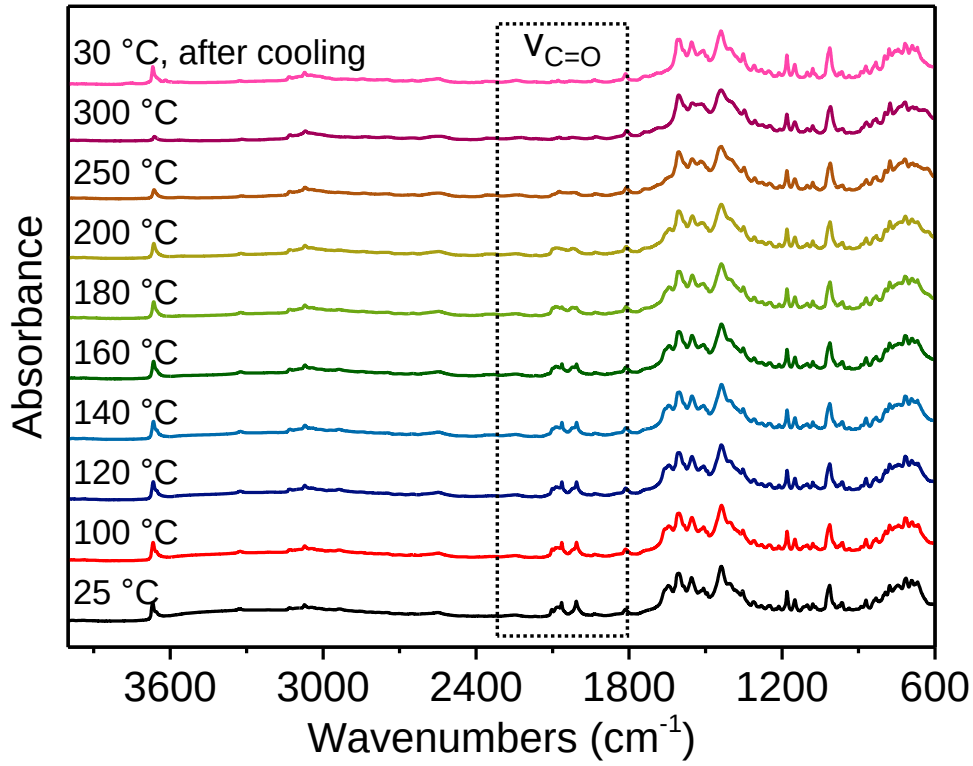

Figure S30. VT-DRIFTS spectra of **Rh/PCN-222** in the range of 4000-600 cm^{-1}.

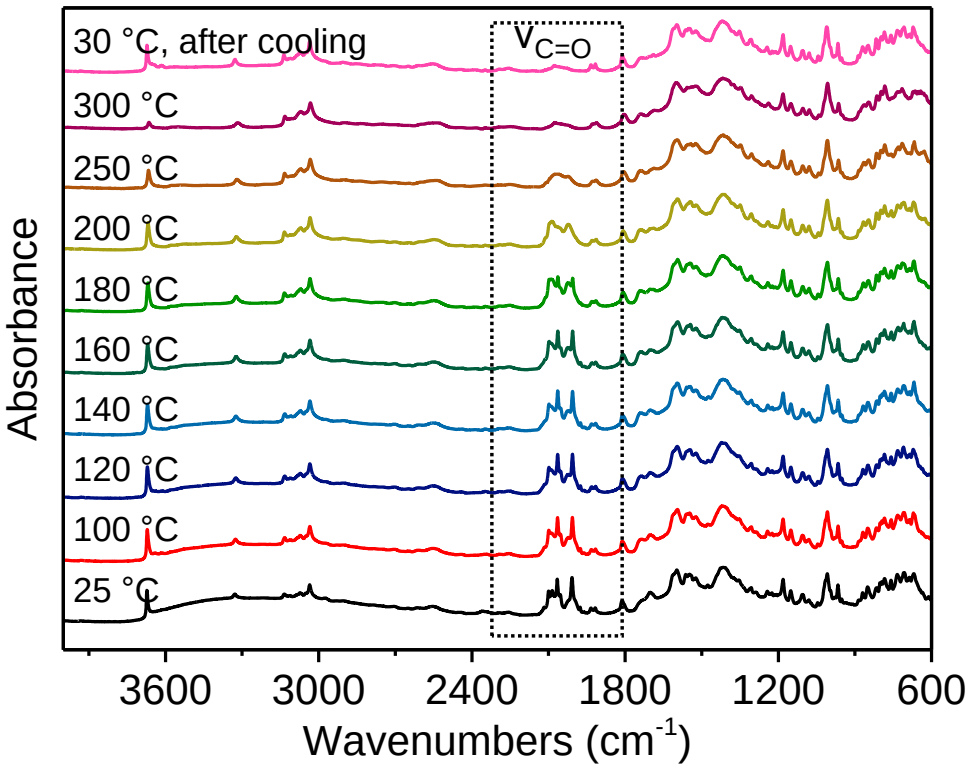

Figure S31. VT-DRIFTS spectra of **Rh/NU-1102** in the range of 4000-600 cm^{-1}.

S4.6. Powder X-ray Diffraction Analysis.

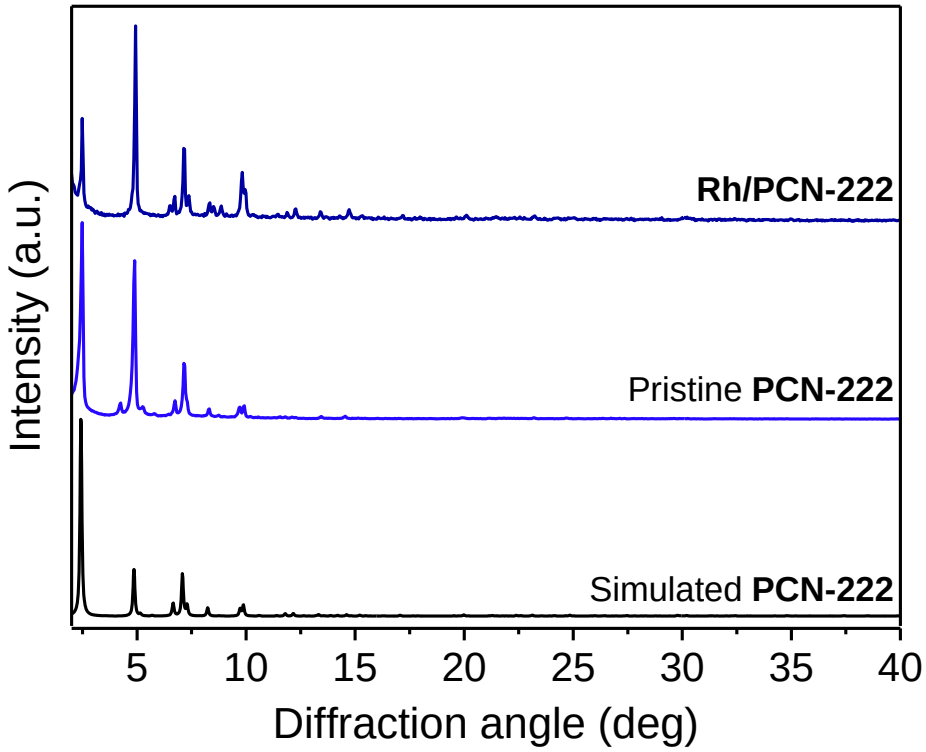

Figure S32. Comparison of PXRD patterns of a bulk sample of: simulated **PCN-222,** pristine **PCN-222** and **Rh/PCN-222**.

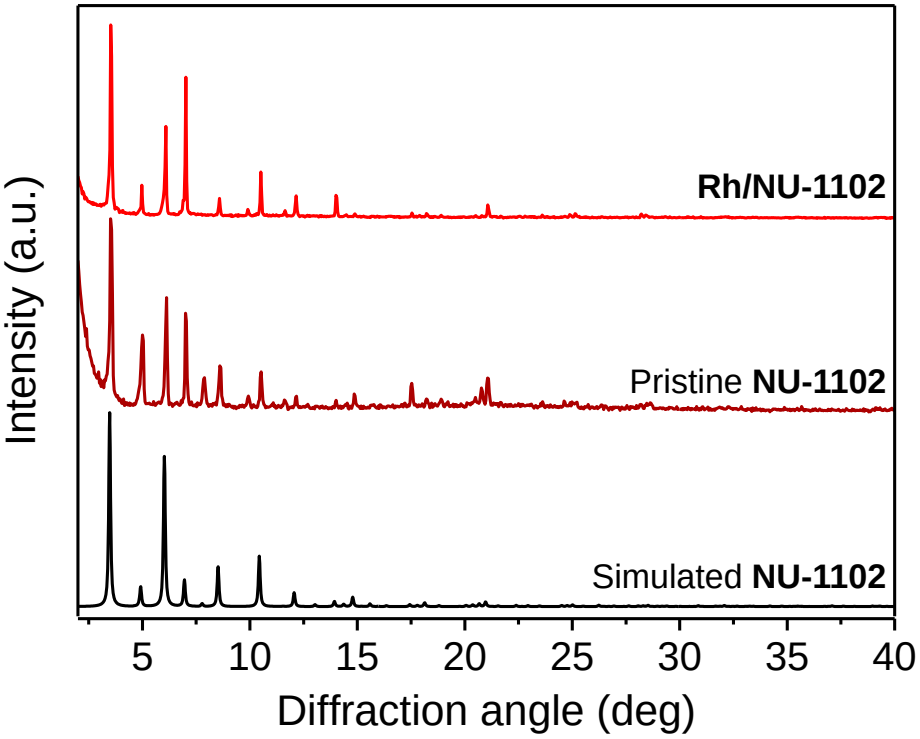

Figure S33. Comparison of PXRD patterns of a bulk sample of: simulated **NU-1102**, pristine **NU-1102** and **Rh/NU-1102**.

S4.7. Thermogravimetric Analysis (TGA).

All performed TGA measurements for Rh/MOFs resulting in ZrO_2 (originating from inorganic node of analyzed material) and Rh_2O_3, remaining as a final product of thermal decomposition. Weight loss observed at the beginning of the TGA curves are associated with the removal of guest solvent molecules. The highest weight loss is caused by the decomposition of the framework which occurs in the temperature range of ca. 350-500 °C. The weight loss calculated from TGA profiles was compared with the theoretical values (shown in the graphs below as values in parentheses).

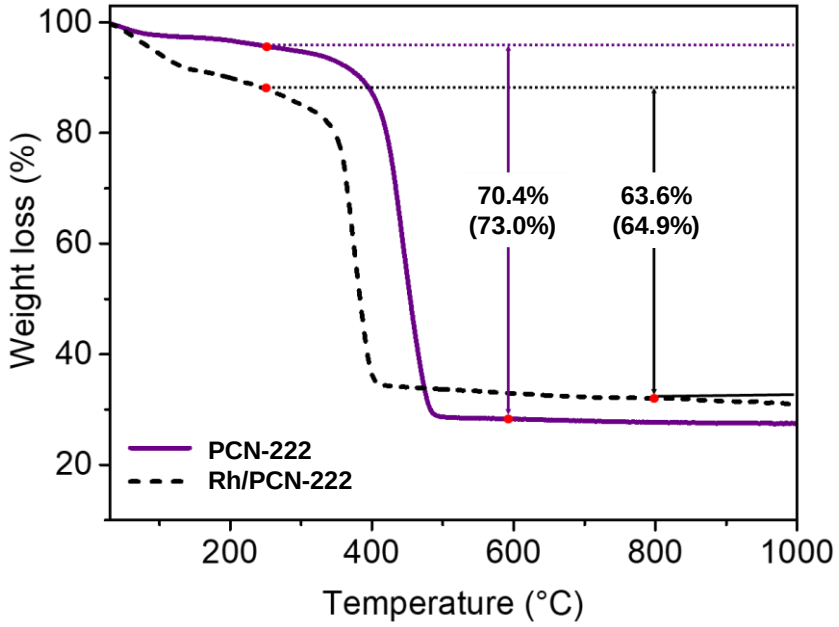

Figure S34. TGA profiles of synthesized samples of **PCN-222** and **Rh/PCN-222** under synthetic air (O_2:N_2 = 20:80) atmosphere.

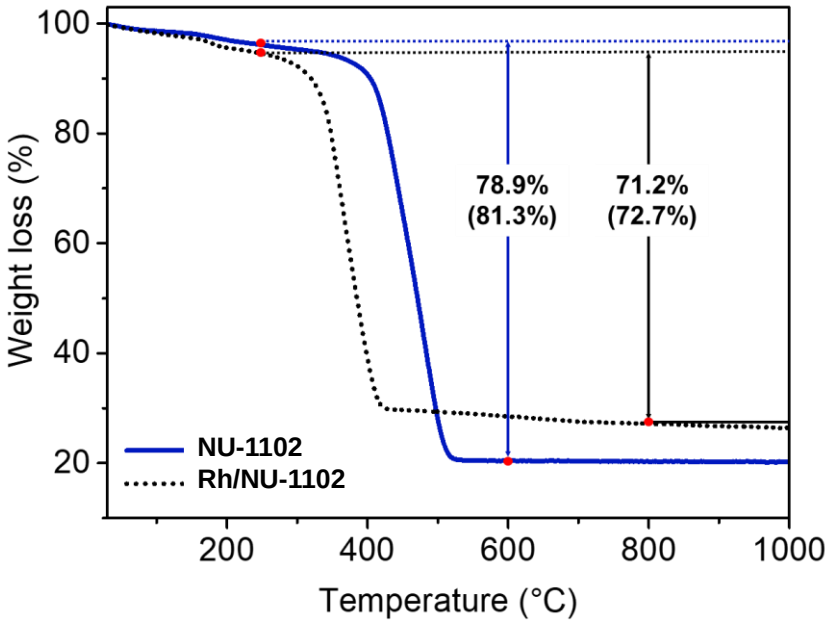

Figure S35. TGA profiles of synthesized samples of **NU-1102** and **Rh/NU-1102** under synthetic air (O_2:N_2 = 20:80) atmosphere.

S4.8. Adsorption of N_2 and BET surface area calculations.

The Brunauer-Emmett-Teller (BET) theory was used to calculate the specific surface areas of obtained materials. For all isotherm analyses we ensured that the two consistency criteria described by Roquerol et al.[5] and Walton et al.[6] were satisfied.

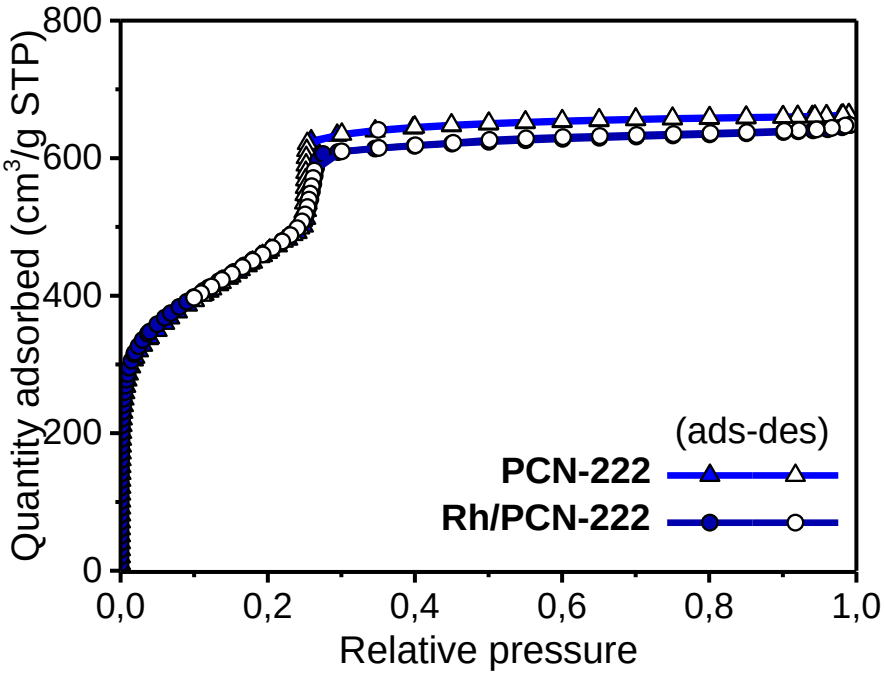

Figure S36. Experimental N_2 adsorption isotherms for **PCN-222** and **Rh/PCN-222** at 77 K (filled symbols - adsorption, open symbols - desorption).

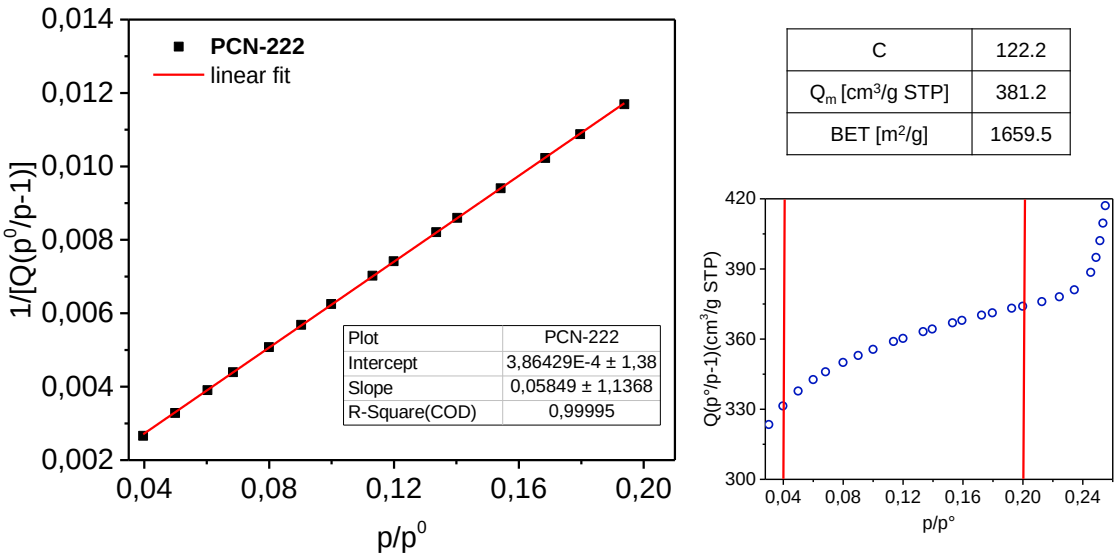

Figure S37. BET plot with parameters (left) and Rouquerol plot (right) for **PCN-222**.

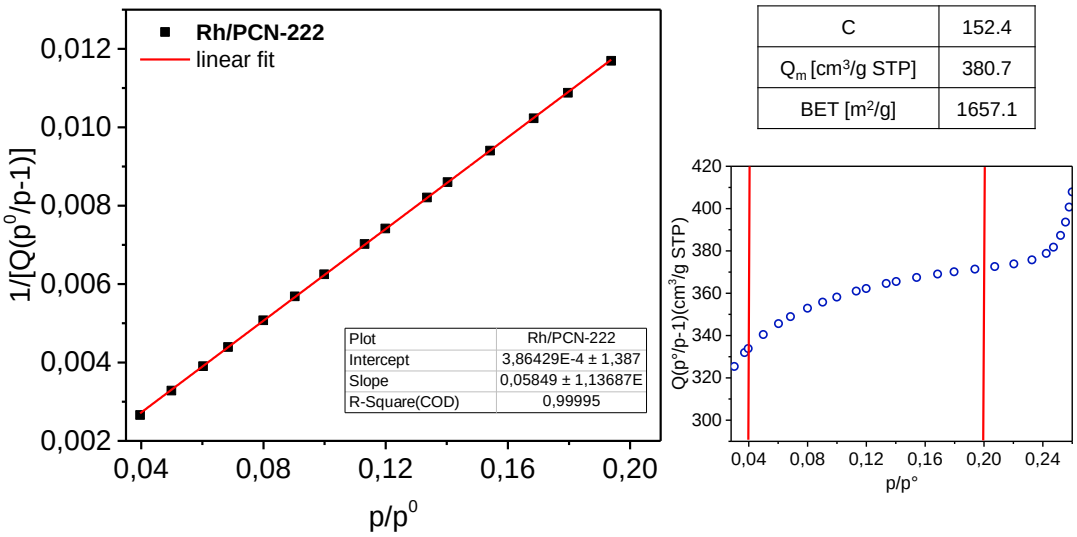

Figure S38. BET plot with parameters (left) and Rouquerol plot (right) for **Rh/PCN-222**.

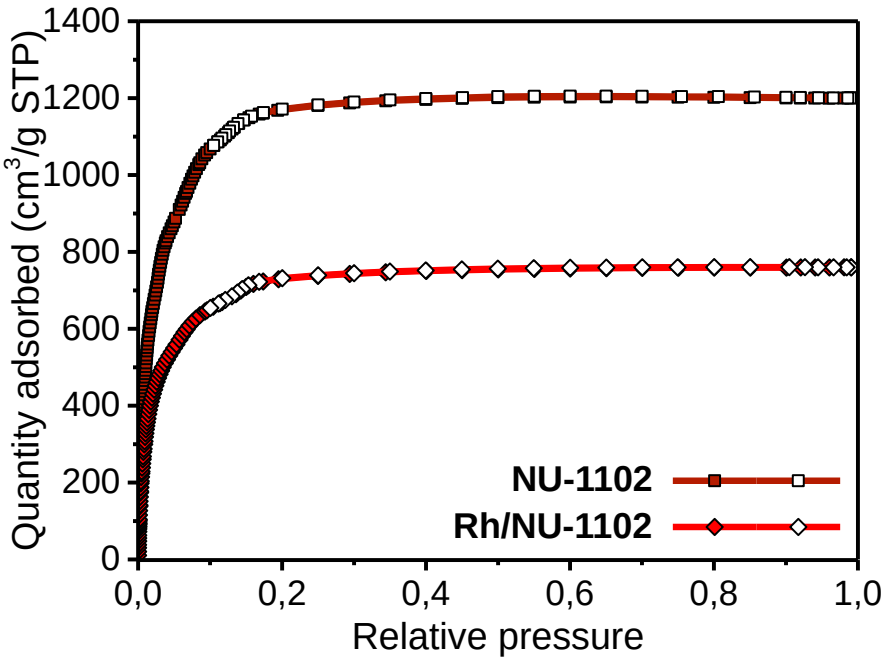

Figure S39. Experimental N_2 adsorption isotherms for **NU-1102** and **Rh/NU-1102** at 77 K (filled symbols - adsorption, open symbols - desorption).

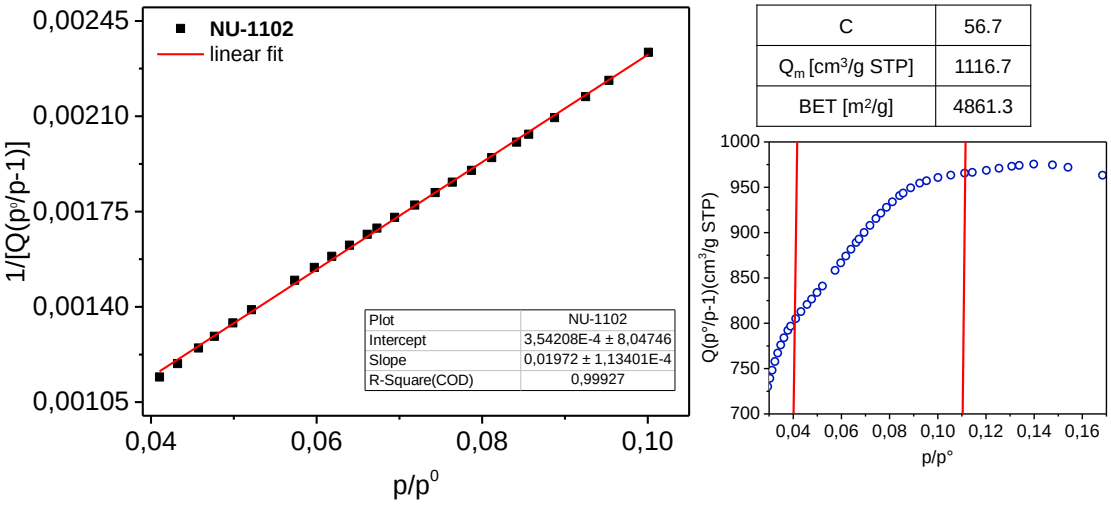

Figure S40. BET plot with parameters (left) and Rouquerol plot (right) for **NU-1102**.

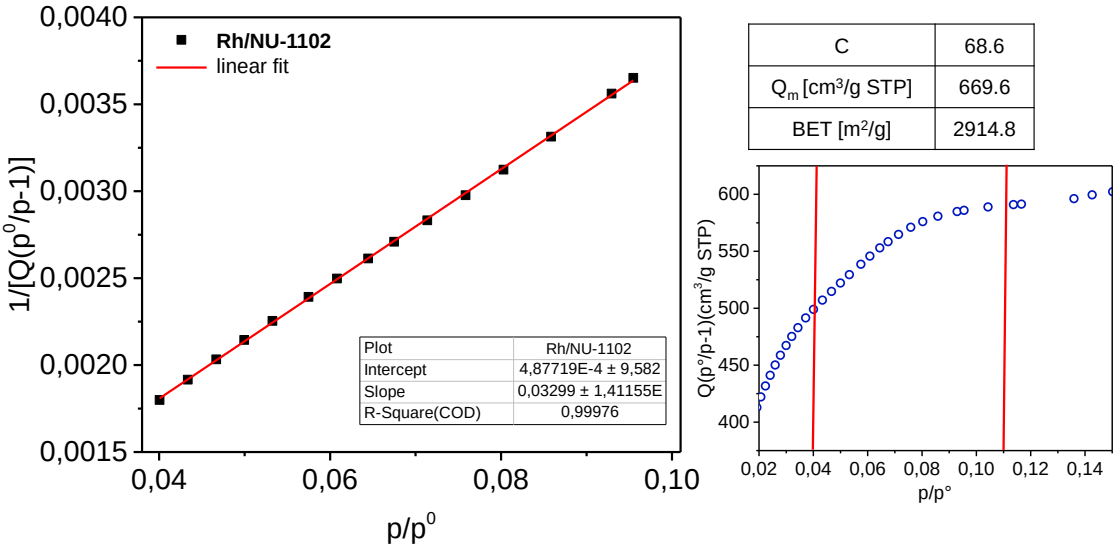

Figure S41. BET plot with parameters (left) and Rouquerol plot (right) for **Rh/NU-1102**.

S5. Hydrogenation of model olefins.

S5.1. General conditions for rhodium catalyst in the hydrogenation of model olefins

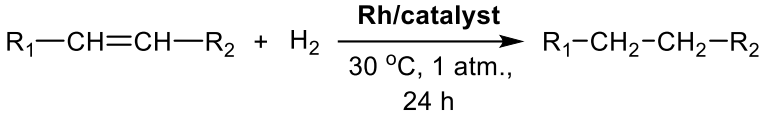

For **Rh/PCN-222**: 0.292 mmol unsaturated hydrocarbon, 4 mg **Rh/PCN-222** (1 mol% Rh), 4 mL solvent, H_2 1 atm., 30 °C, 24 h.

For **Rh/NU-1102**: 0.307 mmol unsaturated hydrocarbon, 4 mg **Rh/NU-1102** (1 mol% Rh), 4 mL solvent, H_2 1 atm., 30 °C, 24 h.

For **1c**: 0.344 mmol unsaturated hydrocarbon, 2 mg **1c** (1 mol% Rh), 4 mL solvent, H_2 1 atm., 30 °C, 24 h.

S5.2. Comparison of kinetic profiles of hydrogenation of selected unsaturated hydrocarbons by Rh/MOFs.

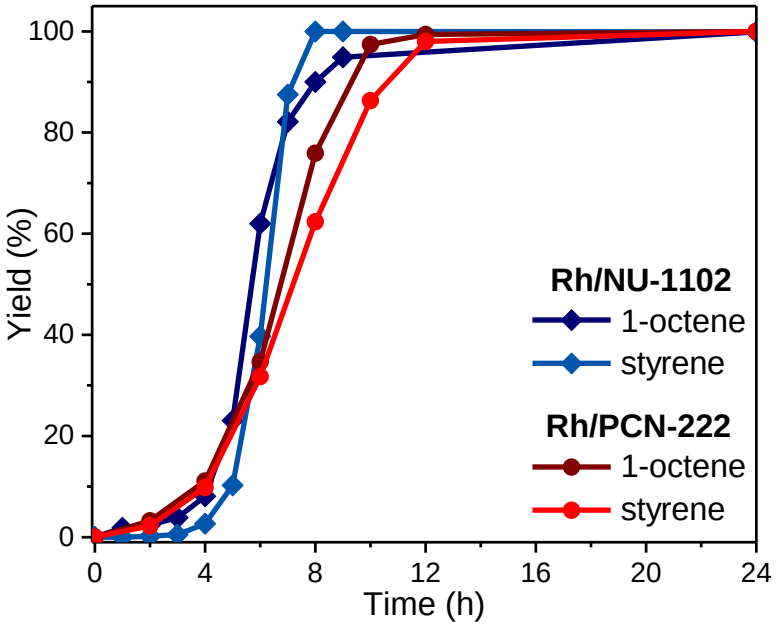

Figure S42. Comparison of kinetic profiles of hydrogenation of selected unsaturated hydrocarbons by **Rh/NU-1102** and **Rh/PCN-222**.

Table S9. Catalytic activity of **Rh/PCN-222**

Entry	alkene	Time (h)	Yield (%)
1	1-octene	2	3
		4	11
		6	35
		8	76
		10	97
		12	99
		24	99
2	styrene	2	2
		4	10
		6	32
		8	62
		10	86
		12	98
		24	99

Table S10. Catalytic activity of **Rh/NU-1102**

Entry	alkene	Time (h)	Yield (%)
1	1-octene	1	1
		2	2
		3	4
		4	8
		5	23
		6	62
		7	82
		8	90
		9	95
		24	99
2	styrene	1	0
		2	0
		3	1
		4	3
		5	10
		6	40
		7	88
		8	99
		9	99
		24	99

S5.3. Recycling test of Rh/PCN-222 in hydrogenation of 1-octene.

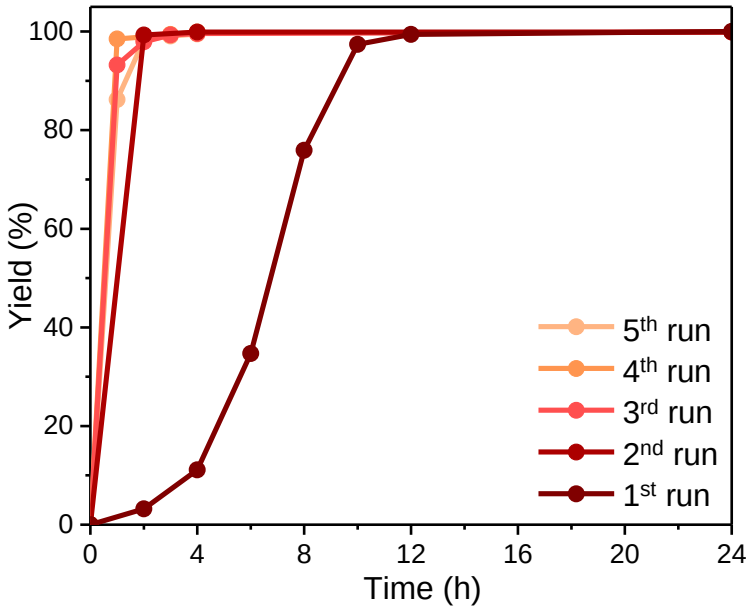

Figure S43. Kinetic profiles of 5 cycles of hydrogenation of 1-octene for **Rh/PCN-222**.

Table S11. Catalytic activity of **Rh/PCN-222** in recycling test

Run	Time (h)	Yield (%)
1	2	3
	4	11
	6	35
	8	76
	10	97
	12	99
	24	99
2	2	97
	4	99
	24	99
3	1	93
	2	98
	3	99
	4	99
	24	99
4	1	99
	2	99
	3	99
	4	99
	24	99
5	1	87
	2	98
	3	99
	4	99
	24	99

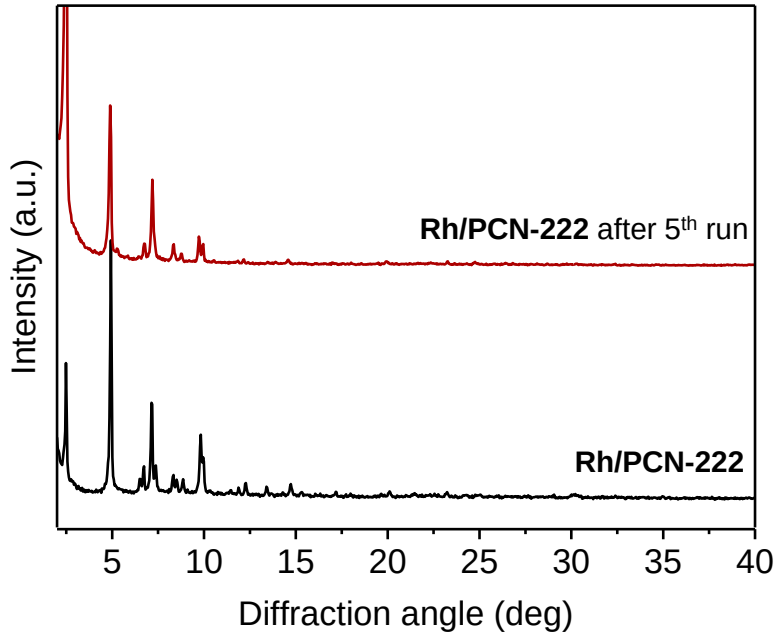

Figure S44. Comparison of PXRD patterns of a bulk sample of **Rh-PCN-222** and **Rh-PCN-222** after 5 runs of hydrogenation.

The PXRD patterns of Rh/PCN-222 before and after all catalytic runs confirmed the retention of the MOF structure.

Table S12. Composition of Rh/MOF analyzed by ICP-OES.

MOF	Rh/Zr (mol/mol)
Rh/PCN-222 (before catalysis)	0.41
Rh/PCN-222 (after catalysis)	0.40
Rh/NU-1102 (before catalysis)	0.58
Rh/NU-1102 (after catalysis)	0.58

S5.4. Effect of solvent and %mol of Rh in hydrogenation of 1-octene by Rh/PCN-222.

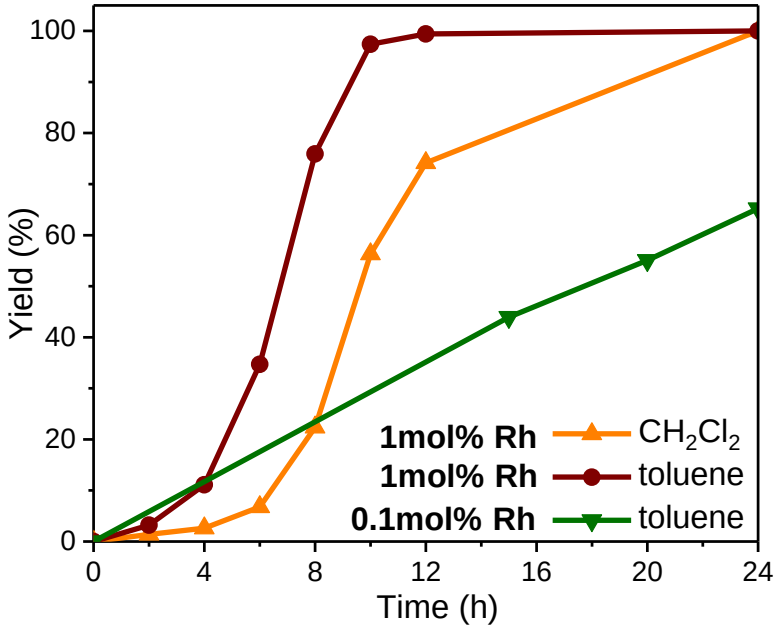

Figure S45. Effect of solvent and %mol of Rh in hydrogenation of 1-octene by **Rh/PCN-222**.

Table S13. Catalytic activity of **Rh/PCN-222** in hydrogenation of 1-octene.

Entry	Solvent	time	Rh content	Yield (%)
1	toluene	2	1 mol%	3
		4		11
		6		35
		8		76
		10		97
		12		99
		24		99
2	CH_2Cl_2	2	1 mol%	2
		4		3
		6		7
		8		22
		10		56
		12		74
		24		100
3	toluene	15	0.1 mol%	44
		20		55
		24		65

S5.5. Effect of water on activation of Rh/PCN-222

Catalytic hydrogenation of 1-octene. To a Schlenk flask with 4 mg of Rh/PCN-222 (0.3 mg, 1 mol% Rh) under N_2 atmosphere a dry toluene (4 mL), water (0.4 µL, 10 mol%) and 1-octene were added (0.3 mmol). Next, the gas phase was removed by short evacuation from the Schlenk flask and H_2 was introduced and left under 1 atm. from a baloon. The resulting mixture was stirred at 30 °C for a limited time in the atmosphere of H_2 (1 atm.). After this time 0.1 mL of solution was collected above the crystals of Rh/MOF, filtered with cotton wool, diluted with 0.5 mL of CH_2Cl_2 and analyzed by using a GC-flame ionization detector.

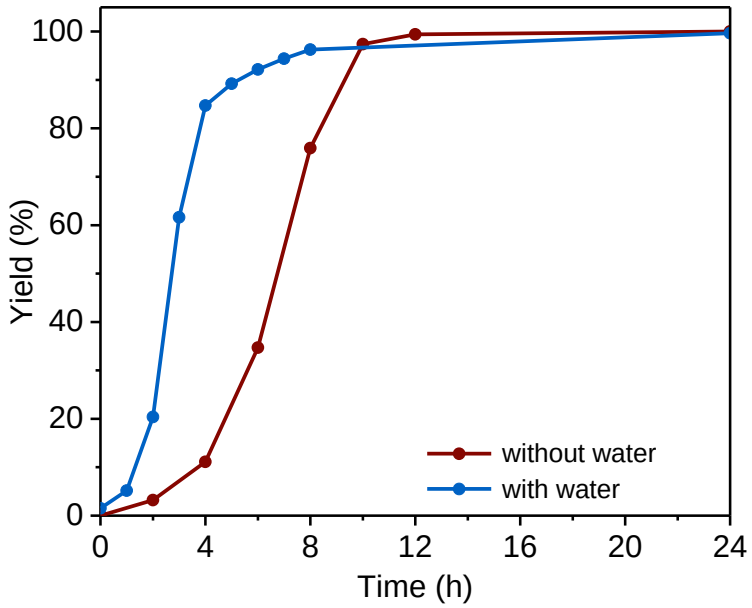

Figure S46. Effect of water addition to the hydrogenation of 1-octene by **Rh/PCN-222**.

S6. Catalyst activation pathway studied by in-situ DRIFTS

S6.1. Interaction of 1c with H_2.

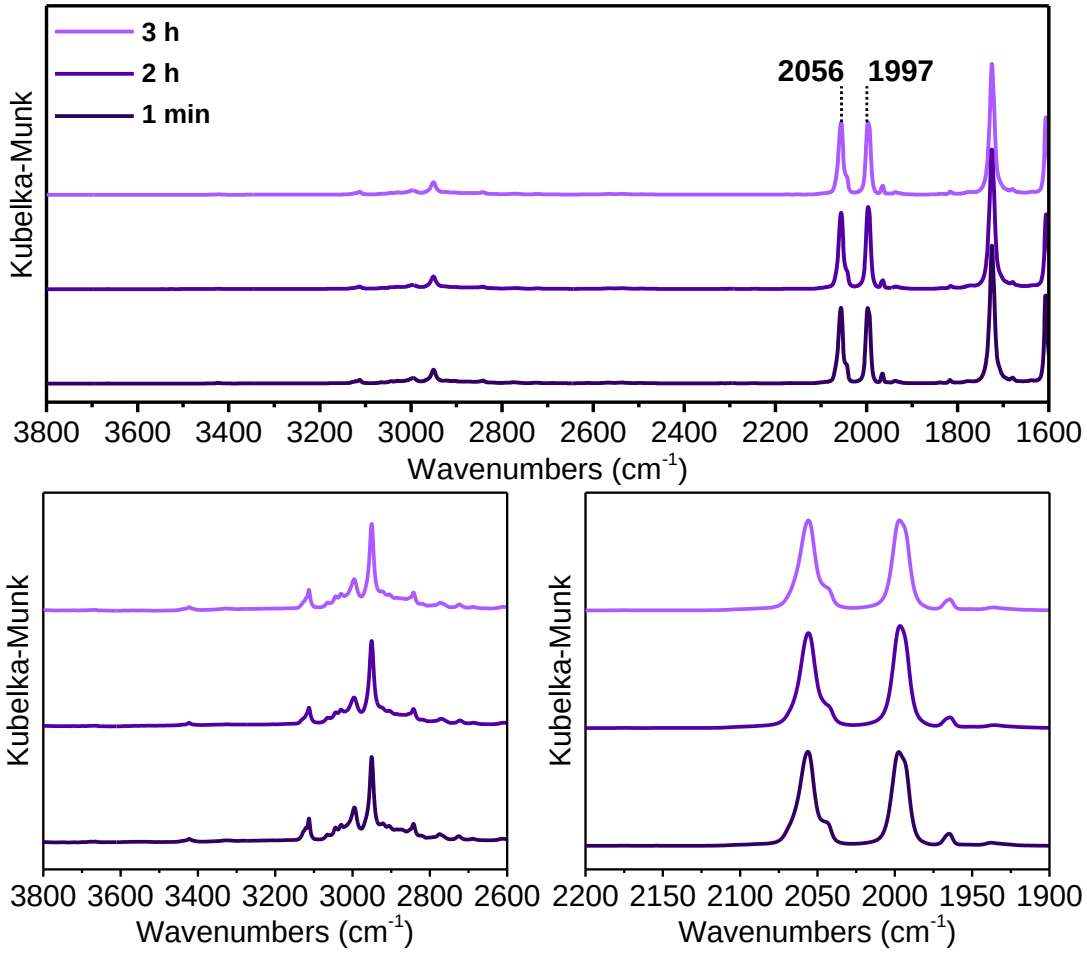

Figure S47. DRIFT spectra of **1c** under H_2 (1 atm.) at 30 °C collected at different time intervals (1 min, 2 h and 3 h).

S6.2. Interaction of Rh/PCN-222 with H_2.

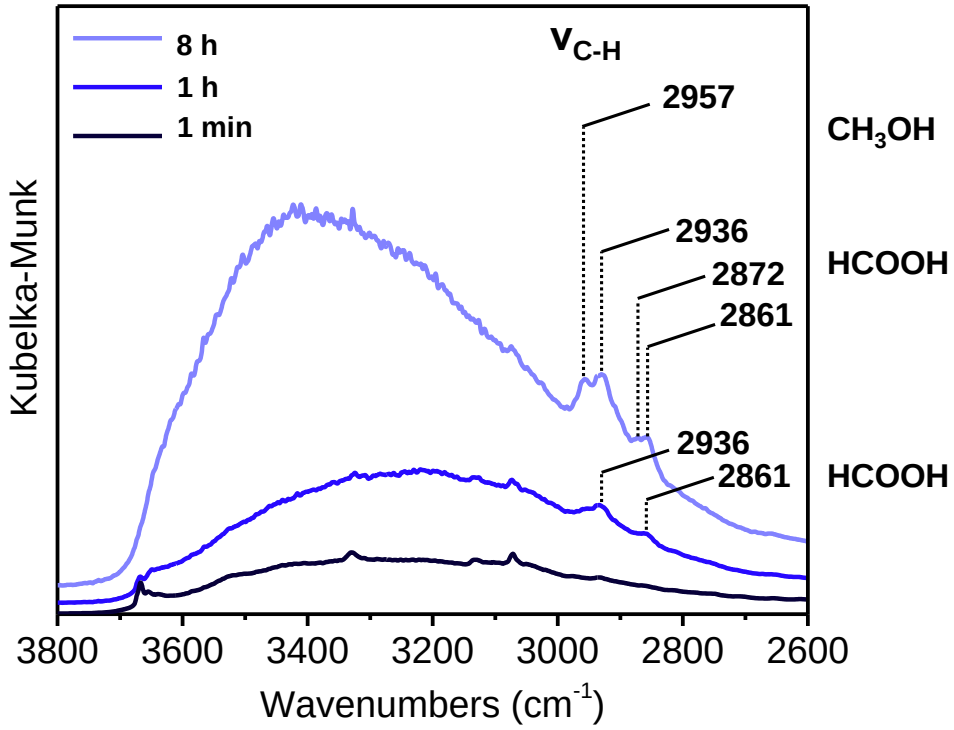

Figure S48. DRIFT spectra of **Rh/PCN-222** with marked bands associated with the vibration of the C-H bond.

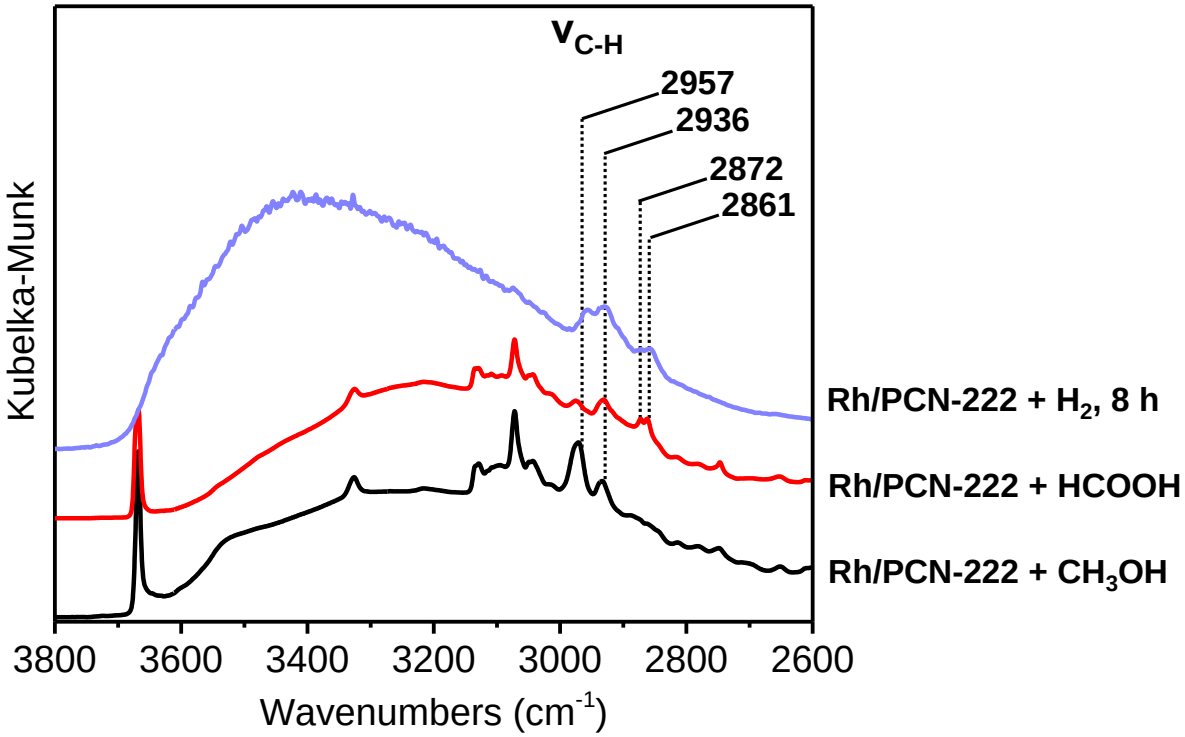

Figure S49. Comparison of DRIFTS spectra of **Rh/PCN-222** and two reference spectra.

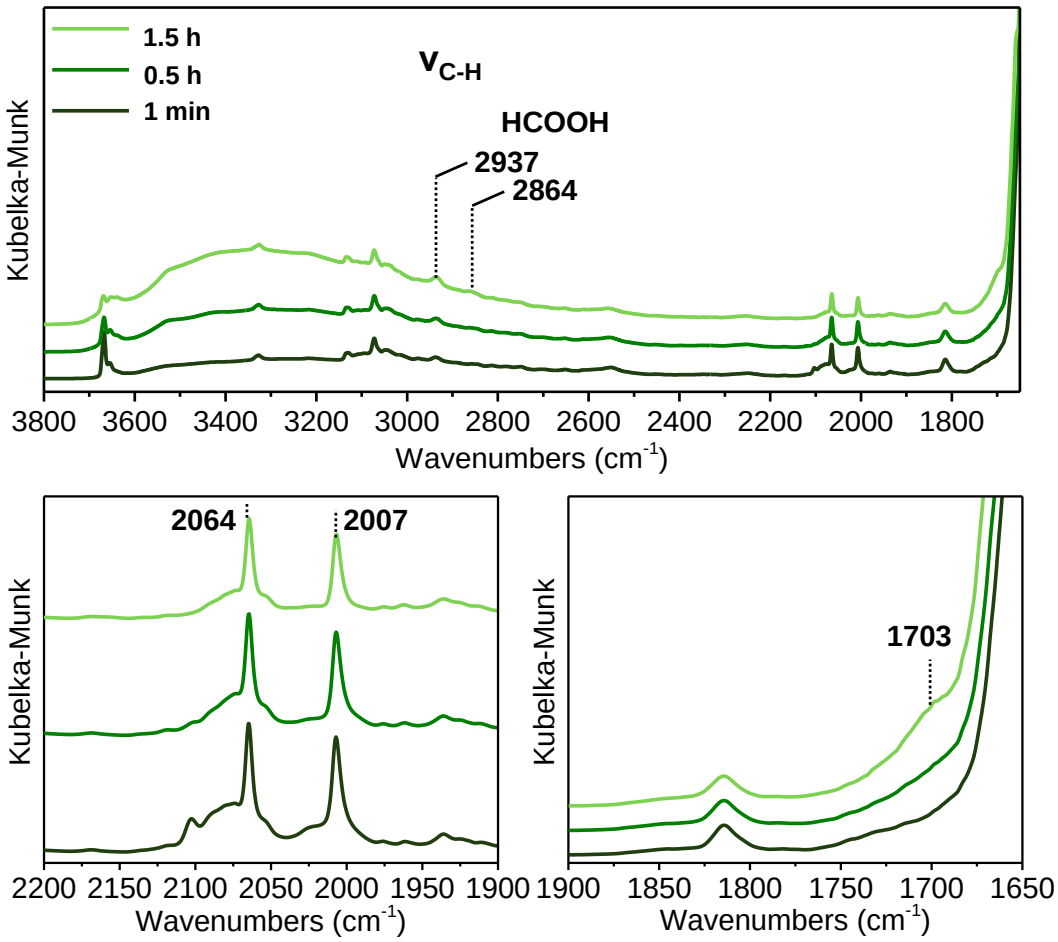

Figure S50. DRIFTS spectra of dried **Rh/PCN-222** after drying the reaction chamber (48 h at 100 °C) under H_2 (1 atm.) at 30 °C.

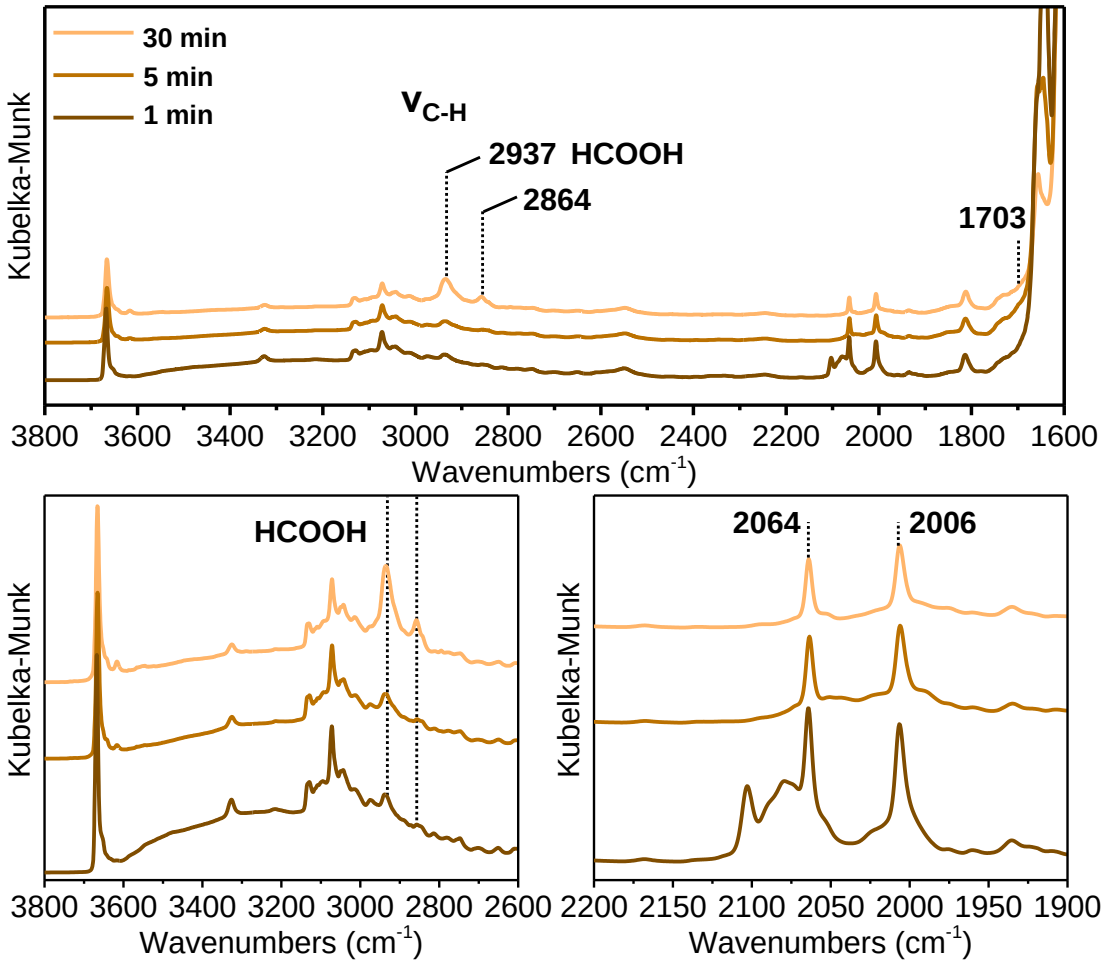

Figure S51. DRIFT spectra of **Rh/PCN-222** at 120 °C.

S6.3. Activation pathway of Rh/NU-1102.

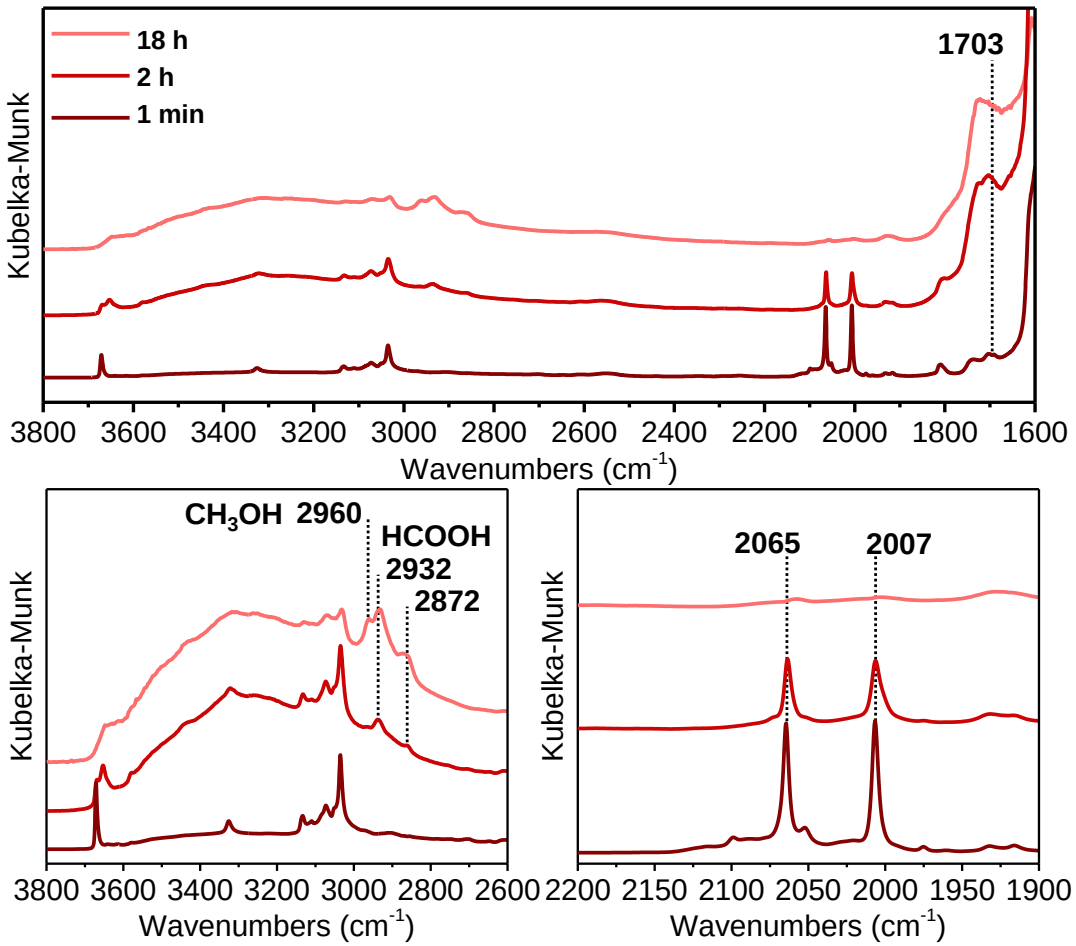

Figure S52. DRIFT spectra of **Rh/NU-1102** at 120 °C.

S6.4. State-of-the-art systems active in hydrogenation of 1-octene or styrene.

Table S14. Hydrogenation of 1-octene and styrene catalyzed by various heterogeneous catalysts.

Lp.	Catalyst	alkene	Reaction conditions	Time [h]	Yield [%]
1	**$[Ru_3(btc)_{1.39}(pydc)_{0.61}Cl_{0.36}] \cdot 2.65AcOH$**	1-octene	50 °C, 7.9 atm H_2, 1 mol% [Ru],	1	99[7]
2	**Pd/C**	1-octene	RT, 7 atm H_2, 0.8 mol% [Pd], ethyl acetate	1	98[8]
3	**Pd/Fe_3O_4@HKUST-1**	1-octene	40 °C, H_2 bubbling (10 mL/min), 3 mol% [Pd], methanol	3	98[9]
4	**Rh/PCN-222**	1-octene	30 °C, H_2 1 atm., 1 mol% [Rh], toluene	12	99*
5	**Rh/PCN-222 after activation**	1-octene	30 °C, H_2 1 atm., 1 mol% [Rh], toluene	1	99*
6	**Rh/NU-1102**	1-octene	30 °C, H_2 1 atm., 1 mol% [Rh], toluene	12	99*
7	**ZJU-28-1a**	1-octene	75 °C, H_2 10 atm., 0.02 mol% [Rh],	24	80[10]
8	**MIL-101-SO_3-1a**	1-octene	75 °C, H_2 10 atm., 0.02 mol% [Rh],	24	80[10]
9	**Sr-AEPF-13**	styrene	60 °C, 5 atm H_2, 1 mol% [Sr], toluene	0.5	99
10	**Pd/C**	styrene	RT, 7 atm H_2, 0.2 mol% [Pd], ethyl acetate	1	43[8]
11	**Rh/PCN-222**	styrene	30 °C, H_2 1 atm., 1 mol% [Rh], toluene	12	99*
12	**Rh/NU-1102**	styrene	30 °C, H_2 1 atm., 1 mol% [Rh], toluene	10	99*
13	**Pd@UiO-67**	styrene	RT, H_2 1 atm., 1 mol% [Pd], THF	1	99[11]
14	**Pd-in-UiO-67**	styrene	RT, H_2 1 atm., 1 mol% [Pd], THF	0.3	99[11]

***** This work

References

(1) Feng, D.; Gu, Z.-Y.; Li, J.-R.; Jiang, H.-L.; Wei, Z.; Zhou, H.-C. Zirconium-Metalloporphyrin PCN-222: Mesoporous Metal–Organic Frameworks with Ultrahigh Stability as Biomimetic Catalysts. *Angew. Chem. Int. Ed.* **2012**, *51* (41), 10307–10310. https://doi.org/10.1002/anie.201204475.

(2) Wang, T. C.; Bury, W.; Gómez-Gualdrón, D. A.; Vermeulen, N. A.; Mondloch, J. E.; Deria, P.; Zhang, K.; Moghadam, P. Z.; Sarjeant, A. A.; Snurr, R. Q.; Stoddart, J. F.; Hupp, J. T.; Farha, O. K. Ultrahigh Surface Area Zirconium MOFs and Insights into the Applicability of the BET Theory. *J. Am. Chem. Soc.* **2015**, *137* (10), 3585–3591. https://doi.org/10.1021/ja512973b.

(3) Ren, Z.; Liu, Y.; Lyu, Y.; Song, X.; Zheng, C.; Feng, S.; Jiang, Z.; Ding, Y. Single-Atom Rh Based Bipyridine Framework Porous Organic Polymer: A High Active and Superb Stable Catalyst for Heterogeneous Methanol Carbonylation. *J. Catal.* **2019**, *369*, 249–256. https://doi.org/10.1016/j.jcat.2018.11.015.

(4) Xue, X.; Yu, J.; Han, Y.; Xiao, X.; Shi, Z.; Mao, H.; Mao, D. Zr-Based Metal–Organic Frameworks Drived Rh–Mn Catalysts for Highly Selective CO Hydrogenation to C_2 Oxygenates. *J. Ind. Eng. Chem.* **2020**, *86*, 220–231. https://doi.org/10.1016/j.jiec.2020.03.008.

(5) Rouquerol, J.; Llewellyn, P.; Rouquerol, F. Is the Bet Equation Applicable to Microporous Adsorbents? In *Studies in Surface Science and Catalysis*; Elsevier, 2007; Vol. 160, pp 49–56. https://doi.org/10.1016/S0167-2991(07)80008-5.

(6) Walton, K. S.; Snurr, R. Q. Applicability of the BET Method for Determining Surface Areas of Microporous Metal−Organic Frameworks. *J. Am. Chem. Soc.* **2007**, *129* (27), 8552–8556. https://doi.org/10.1021/ja071174k.

(7) Kozachuk, O.; Luz, I.; Llabrés i Xamena, F. X.; Noei, H.; Kauer, M.; Albada, H. B.; Bloch, E. D.; Marler, B.; Wang, Y.; Muhler, M.; Fischer, R. A. Multifunctional, Defect-Engineered Metal-Organic Frameworks with Ruthenium Centers: Sorption and Catalytic Properties. *Angew. Chem. Int. Ed.* **2014**, *53* (27), 7058–7062. https://doi.org/10.1002/anie.201311128.

(8) Hwang, C.-B.; Fu, Y.-S.; Lu, Y.-L.; Jang, S.-W.; Chou, P.-T.; Wang, C. R. C.; Yu, S. J. Synthesis, Characterization, and Highly Efficient Catalytic Reactivity of Suspended Palladium Nanoparticles. *J. Catal.* **2000**, *195* (2), 336–341. https://doi.org/10.1006/jcat.2000.2992.

(9) Guarnizo, A.; Angurell, I.; Rossell, M. D.; Llorca, J.; Muller, G.; Seco, M.; Rossell, O. 4-Mercaptophenyldiphenylphosphine as Linker to Immobilize Pd onto the Surface of Magnetite Nanoparticles. Excellent Catalytic Efficiency of the System after Partial Linker Removal. *RSC Adv.* **2015**, *5* (111), 91340–91348. https://doi.org/10.1039/C5RA18953E.

(10) Genna, D. T.; Pfund, L. Y.; Samblanet, D. C.; Wong-Foy, A. G.; Matzger, A. J.; Sanford, M. S. Rhodium Hydrogenation Catalysts Supported in Metal Organic Frameworks: Influence of the Framework on Catalytic Activity and Selectivity. *ACS Catal.* **2016**, *6* (6), 3569–3574. https://doi.org/10/gddsz8.

(11) Chen, L.; Chen, X.; Liu, H.; Bai, C.; Li, Y. One-Step Encapsulation of Pd Nanoparticles in MOFs via a Temperature Control Program. *J. Mater. Chem. A* **2015**, *3* (29), 15259–15264. https://doi.org/10.1039/C5TA02860D.